AD-A032 991 ARMY ENGINEER WATERWAYS EXPERIMENT STATION VICKSBURG MISS F/G 8/3
EFFECT OF SOURCE ORIENTATION AND LOCATION IN THE PERU-CHILE TRE--ETC(U)
SEP 76 A W GARCIA

UNCLASSIFIED WES-RR-H-76-2 NL

| OF |
AD
A032991

END

DATE
FILMED
1-77

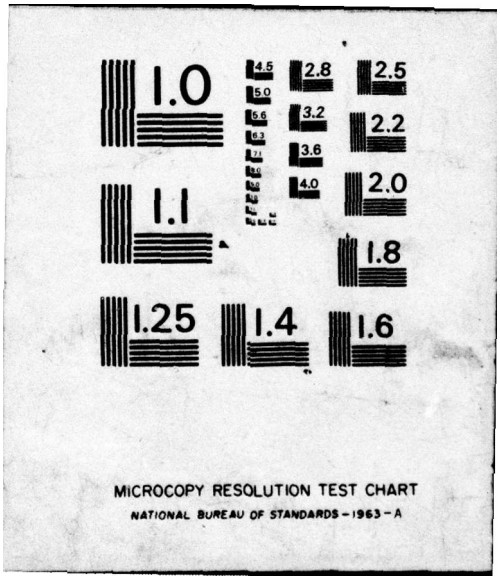
1.0
1.1
1.25
1.4
1.6
1.8
2.0
2.2
2.5
2.8
3.2
3.6
4.0
4.5
5.0
5.6
6.3
MICROCOPY RESOLUTION TEST CHART
NATIONAL BUREAU OF STANDARDS - 1963 - A

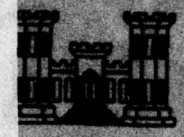

RESEARCH REPORT H-76-2

EFFECT OF SOURCE ORIENTATION AND LOCATION IN THE PERU-CHILE TRENCH ON TSUNAMI AMPLITUDE ALONG THE PACIFIC COAST OF THE CONTINENTAL UNITED STATES

by

Andrew W. Garcia

Hydraulics Laboratory
U. S. Army Engineer Waterways Experiment Station
P. O. Box 631, Vicksburg, Miss. 39180

September 1976
Final Report

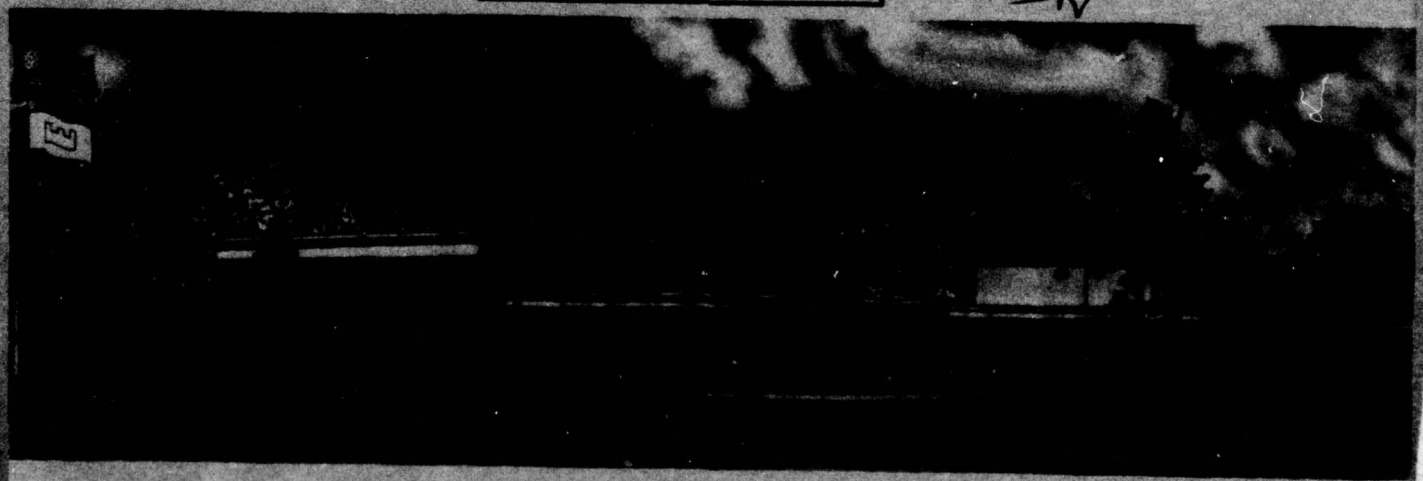

Prepared for Office, Chief of Engineers, U. S. Army
Washington, D. C. 20314

Destroy this report when no longer needed. Do not return it to the originator.

(14) WES-RR-H-76-2

Unclassified

SECURITY CLASSIFICATION OF THIS PAGE (When Data Entered)

REPORT DOCUMENTATION PAGE	READ INSTRUCTIONS BEFORE COMPLETING FORM
1. REPORT NUMBER: Research Report H-76-2	2. GOVT ACCESSION NO. / 3. RECIPIENT'S CATALOG NUMBER
4. TITLE (and Subtitle): (6) EFFECT OF SOURCE ORIENTATION AND LOCATION IN THE PERU-CHILE TRENCH ON TSUNAMI AMPLITUDE ALONG THE PACIFIC COAST OF THE CONTINENTAL UNITED STATES.	5. TYPE OF REPORT & PERIOD COVERED: (9) Final report. / 6. PERFORMING ORG. REPORT NUMBER
7. AUTHOR(s): (10) Andrew W. Garcia	8. CONTRACT OR GRANT NUMBER(s)
9. PERFORMING ORGANIZATION NAME AND ADDRESS: U. S. Army Engineer Waterways Experiment Station, Hydraulics Laboratory, P. O. Box 631, Vicksburg, Mississippi 39180	10. PROGRAM ELEMENT, PROJECT, TASK AREA & WORK UNIT NUMBERS: Work Unit 31093
11. CONTROLLING OFFICE NAME AND ADDRESS: Office, Chief of Engineers, U. S. Army, Washington, D. C. 20314	12. REPORT DATE: September 1976 (11) Sep 76 / 13. NUMBER OF PAGES: 44 (12) 48p.
14. MONITORING AGENCY NAME & ADDRESS (if different from Controlling Office)	15. SECURITY CLASS. (of this report): Unclassified / 15a. DECLASSIFICATION/DOWNGRADING SCHEDULE

16. DISTRIBUTION STATEMENT (of this Report)

Approved for public release; distribution unlimited.

17. DISTRIBUTION STATEMENT (of the abstract entered in Block 20, if different from Report)

18. SUPPLEMENTARY NOTES

19. KEY WORDS (Continue on reverse side if necessary and identify by block number)

Finite difference method
Pacific Coast
Peru-Chile Trench
Tsunamis

20. ABSTRACT (Continue on reverse side if necessary and identify by block number)

An idealized axis of the Peru-Chile Trench was divided into 12 segments of equal length. A hypothetical bottom displacement which generates a tsunami with intensity approximately equal to four was centered in three of the segments. An explicit finite difference numerical code was used to simulate generation and propagation of the resulting tsunami to the west coast of the continental United States. Additionally, the tsunami of 22 May 1960 was simulated and comparison made to gage records at selected open coast locations

(Continued)

CONT. ON NEXT P.

DD FORM 1 JAN 73 1473 EDITION OF 1 NOV 65 IS OBSOLETE

Unclassified

SECURITY CLASSIFICATION OF THIS PAGE (When Data Entered)

20. ABSTRACT (Continued).

along the U. S. Pacific coast. Contour plots of surface elevation of the few leading waves of the tsunami at selected times are presented. An analytical technique is used to normalize the amplitude of the leading wave of the tsunami to its amplitude at 600-ft water depth. For purposes of comparison, the amplitudes of the tsunamis generated in each segment are plotted as a function of distance along the Pacific coast from the Mexican to the Canadian border. These plots allow an evaluation of the relative vulnerability of coastal locations to tsunamis generated in different locations of the Peru-Chile Trench.

PREFACE

Authority for the U. S. Army Engineer Waterways Experiment Station (WES) to conduct this study, Work Unit No. 31093, "Harbor Design Criteria for Tsunami Protection," under the Corps of Engineers Research and Development Program was contained in a letter from the Office, Chief of Engineers (OCE), U. S. Army, dated 17 September 1973. Funds were granted by the Coastal Engineering Research Area under the field managership of the Coastal Engineering Research Center and OCE Technical Monitor, Mr. Neill Parker, HQDA (DAEN-CWE-H).

The study was conducted by personnel of the Hydraulics Laboratory, WES, under the direction of Mr. H. B. Simmons, Chief of the Hydraulics Laboratory, Dr. R. W. Whalin, Chief of the Wave Dynamics Division, and Mr. D. D. Davidson, Chief of the Wave Research Branch. The investigation was conducted by Messrs. A. W. Garcia and H. L. Butler. This report was prepared by Mr. Garcia.

Most of the numerical computations were performed on a CDC-7600 computer at the Los Alamos Scientific Laboratory, Los Alamos, New Mexico.

Directors of WES during the investigation and the preparation and publication of this report were COL G. H. Hilt, CE, and COL John L. Cannon, CE. Technical Director was Mr. F. R. Brown.

CONTENTS

CONVERSION FACTORS, U. S. CUSTOMARY TO METRIC (SI) AND METRIC (SI) TO U. S. CUSTOMARY UNITS OF MEASUREMENT

Units of measurement used in this report can be converted as follows:

Multiply	By	To Obtain
U. S. Customary to Metric (SI)		
feet	0.3048	metres
miles (U. S. statute)	1.609344	kilometres
degrees (angle)	0.01745329	radians
Metric (SI) to U. S. Customary		
centimetres	0.3937007	inches
metres	3.280839	feet

EFFECT OF SOURCE ORIENTATION AND LOCATION IN THE PERU-CHILE TRENCH ON TSUNAMI AMPLITUDE ALONG THE PACIFIC COAST OF THE CONTINENTAL UNITED STATES

PART I: INTRODUCTION

Purpose of Study

1. The U. S. Army Corps of Engineers has as an objective of its research and development program the determination of better harbor design criteria for tsunami protection. A previous report[1] discussed the subject of tsunami vulnerability of the Pacific coast of the continental United States to tsunamis originating in the Aleutian Trench. That report determined the variation in tsunami amplitude as a function of coastal distance due to a standard uplift source at different locations in the Aleutian Trench. This report is a continuation of that study and addresses the subject of tsunami vulnerability along the same stretch of coast to tsunamis originating in the Peru-Chile Trench. In addition, modifications to the numerical code used in the previous report allowed the simulation of the Chilean tsunami of 22 May 1960.

Historical Narrative

2. Five well-documented major tsunamis have struck the Pacific coast of the United States in recent times: the Great Aleutian tsunami of 1946, the Kamchatka tsunami of 1952, the Alaskan tsunami of 1957, the Chilean tsunami of 1960, and the Alaskan tsunami of 1964. The 1964 Alaskan tsunami claimed 107 lives in Alaska, 4 in Oregon, and 11 in Crescent City, California. In addition to 330 lives in Chile, the 1960 Chilean tsunami claimed 61 in Hawaii and 199 in Japan.

3. The association of large submarine earthquakes with island arcs and deep submarine trenches is well documented.[2-4] The Japan-Kurile-Kamchatka, the Aleutian, and the Peru-Chile Trench regions have long recorded histories of tsunamigenic activity. Of these, however,

only tsunamis originating in the Aleutian and Peru-Chile Trenches have a history of causing significant runup along the Pacific coast of the United States. Because tsunamis originating in the Aleutian Trench is the subject of a previous report,[1] it will not be recounted here.

4. On 9 July 1586 a tsunami occurred in the vicinity of Lima, Peru. Waves as high as 84 ft* and inundation as far inland as 6 miles were reported. On 28 October 1746 the city of Callao, Peru, was destroyed by two waves; reportedly, only 200 of 5000 inhabitants survived. On 20 February 1835 a major quake was felt throughout Chile. A 50-ft wave was reported at Talcahuano and ships were sunk in the port of Constitucion. Waves were reported as far away as Hawaii. On 13 August 1868 a large shock was reported centered near Arica, Peru. The city of Iquique was reported inundated and waves rising 30 ft above high tide were reported at Talcahuano. On 11 November 1922 a major quake was reported near Coquimbo where three waves reached 1-1/4 miles inland. Destructive waves were reported from Japan, Formosa, the Philippines, and Hawaii. On 19 January 1958 a large earthquake of magnitude 7.5 was reported centered near 1-1/2°N, 79-1/2°W. Tsunamis causing damage were reported at Las Esmeraldas and Guayaquil, Ecuador, with 20 killed and many injured.[5] The tsunami of 22 May 1960 is described as one of the largest of the past century. Table 1 (adapted from Symons and Zetler[6] shows a comparison of maximum wave heights for the tsunamis of 1946, 1952, 1957, 1960, and 1964. The comparative intensity of the 1960 tsunami is evident, especially when distance effects are considered; indeed, the generating earthquake was of magnitude 8.6, one of the largest ever recorded.

5. There is some evidence, however, to indicate that Richter scale magnitudes tend to underestimate source parameters (fault length, width, and uplift) and thus the tsunamigenic potential of very large earthquakes. Cumulative frequency versus surface wave magnitude (M_s)**

---

* A table of factors for converting U. S. customary units of measurement to metric (SI) units and metric (SI) units to U. S. customary is presented on page 3.

** For convenience, symbols and unusual abbreviations are listed and defined in the Notation (Appendix A).

plots show a linear trend for earthquakes with M_s values less than about 7.0; but for higher values of M_s the locus becomes increasingly steep, tending toward vertical at M_s approximately equal to 8.6. Therefore, it has been commonly assumed that earthquakes with M_s values greater than about 8.6 do not occur, which may indeed be true. This, however, does not necessarily imply there is an upper limit on earthquake source parameters. Conventional analyses of earthquake energy spectra to determine M_s values are frequency-dependent. Chinnery and North[7] hypothesize that because very large earthquakes produce spectra which have significant proportions of energy at frequencies below the band where M_s is normally measured and have dislocations which propagate for times significantly greater than 20 sec, an upper limit to M_s will be observed no matter how large the true earthquake size.

PART II: PERU-CHILE TRENCH AS A TSUNAMIGENIC REGION

6. In terms of plate tectonics, the shallow seismic zone of western South America is a continuous boundary along which one plate (the Nazca plate) underthrusts the adjacent plate (the Americas plate). Kelleher[2] cites numerous studies that indicate this plate motion is accomplished by large magnitude earthquakes; consequently, any segment of the boundary that has not ruptured for many decades should be considered a zone of high risk. Moreover, Kelleher[3] has observed that about once each century the entire fault segment near the Central Valley province of central and southern Chile (approximately 32° to 46°S) has fractured in a general north-south direction by a progression of large earthquakes and hypothesizes that a new series of quakes might start about the end of this century near Valparaiso (33°S) and progress southward.

7. Hayes[8] states that crustal thinning beneath the trench is evidence that the major tectonic forces involved are not laterally compressive, and the absence of these compressive forces can be produced by a combination of faulting and flexure in the transition region of an ocean-continent margin. Hayes also observes that almost all quake epicenters in the area lie shoreward of the axis of the trench.

8. Records kept by the Japanese suggest that the subsea tectonic displacement of the 1960 Chilean earthquake is probably greater than that associated with any of the earlier earthquakes during a period of nearly 500 years.[9] Indeed, vertical movements of a larger regional scale appear to be characteristic of that portion of the trench extending from Colombia to southern Chile. The great earthquake of 1835 (paragraph 4) is reported to have caused uplifts of as much as 8.6 ft at coastal locations extending from Isla Mocha to Concepcion.

PART III: TSUNAMI SOURCE CHARACTERISTICS

9. Figure 1 shows the contours of elevation of the initial sea surface deformation used as input to the simulation of the Chilean tsunami of 22 May 1960. The shape of the deformation is inferred from the works of Plafker and Savage[9] and Hwang et al.[10] Plafker and Savage show the maximum upward vertical displacement of their preferred interpretation of the fault model to be about 10 m (32.8 ft) although the maximum observed upward vertical displacement was about 6 m (19.7 ft). To avoid distorting the large-scale features, the available data were smoothed, i.e., the maximum vertical uplift of 24 ft was chosen to compromise between the maximum predicted uplift of 10 m (32.8 ft) and maximum observed uplift of 6 m (19.7 ft). Because the data indicate there was little downthrow (less than 2 m (6.6 ft)) associated with the tectonic deformation, this feature was neglected in the model. The length of the deformation was determined from the spatial distribution of the epicenters of the initial quake and aftershocks as shown in Plafker and Savage,[9] and both its meridional and latitudinal extent are consistent with the area of the rupture zone as shown in Figure 2.[3]

10. There is little question that the deformation used for the simulation of the 1960 Chilean tsunami is not known with the confidence of that used to simulate the Alaskan tsunami of 28 March 1964. Nonetheless, enough data are available to credibly reconstruct the bottom deformation which generated the tsunami.

11. Figure 3 shows the idealized axis of the Peru-Chile Trench as divided into 12 segments. A hypothetical sea surface deformation which generates a tsunami with intensity approximately equal to four is centered in and aligned with segments 1, 8, and 12. In order to facilitate comparison with the results of a previous study,[1] the present hypothetical uplift is identical with that of the referenced study.

PART IV: COMPUTATIONAL MODEL

Equations of Motion

12. The numerical code used to simulate the 1960 Chilean tsunami and the idealized hypothetical disturbances is based upon the linearized long-wave equations obtained by vertically integrating the Navier-Stokes equations and equation of continuity. The equations as used in the code are formulated in a spherical system as follows:

$$\frac{\partial U}{\partial t} = - \frac{g}{R_e} \frac{\partial \eta}{\partial \theta} \tag{1}$$

$$\frac{\partial V}{\partial t} = - \frac{g}{R_e \sin \phi} \frac{\partial \eta}{\partial \phi} \tag{2}$$

$$\frac{\partial \eta}{\partial t} = \frac{-1}{R_e \sin \phi} \left[\frac{\partial}{\partial \theta} (\eta + d) U \sin \theta + \frac{\partial}{\partial \phi} (\eta + d) V \right] \tag{3}$$

where

U = depth-averaged wave velocity component in the θ direction

t = time

g = acceleration due to gravity

R_e = radius of the earth

η = wave elevation from reference water level

θ = latitude measured positive from north pole

V = depth-averaged wave velocity component in the ϕ direction

ϕ = longitude measured positive eastward from Greenwich

d = local water depth

The validity of using linearized equations and the conditions under which they hold are discussed in Reference 1.

Finite Difference Computational Scheme

13. In order to facilitate simulation of the tsunami of

22 May 1960, modifications were made to the code used for previous reports[1,11,12] to permit larger grids and faster execution. In the above-mentioned reports the finite difference forms of Equations 1, 2, and 3 were solved by an alternating direction multistep technique whereby during the first half-time step, η and U were computed implicitly along lines of constant longitude and V explicitly along lines of constant latitude; in the second half-time step, η and V were computed implicitly along line of constant latitude and U explicitly along lines of constant longitude. In the present report, Equations 4-6 are the finite difference forms of Equations 1-3.

$$U_{i,j}^{n+1/2} = U_{i,j}^{n-1/2} - \frac{g\Delta t}{R_e \Delta\theta} \left(\eta_{i,j} - \eta_{i,j}\right)^n \tag{4}$$

$$V_{i,j}^{n+1/2} = V_{i,j}^{n-1/2} - \frac{g\Delta t}{R_e \Delta\phi \sin\theta} \left(\eta_{i,j+1} - \eta_{i,j}\right)^n \tag{5}$$

$$\eta_{i,j}^{n+1} = \eta_{i,j}^{n} - \frac{1}{R_e \sin\theta} \left\{ \frac{\Delta t}{\Delta\theta} \left[(Ud \sin\theta)_{i,j} - (Ud \sin\theta)_{i-1,j} \right]^{n+1/2} + \frac{\Delta t}{\Delta\phi} \left[(Vd)_{i,j} - (Vd)_{i,j-1} \right]^{n+1/2} \right\} \tag{6}$$

(where it is assumed $\eta << d$)

Figure 4 shows the grid scheme used. The depth, d, is considered the averaged depth over the grid square j to $j+1$, i to $i+1$. Equations 4 and 5 are solved explicitly at the same half-time step along lines of constant longitude and latitude, respectively. Equation 6 is then solved for η one half-time step later. The boundary conditions, reflective at land boundaries and transmissive at the open ocean grid boundaries, are treated in the same manner as in Reference 1.

14. The explicit code was verified by comparing the results of hindcasting the Alaskan tsunami of 28 March 1964 with results of hindcasting the same tsunami using the earlier implicit-explicit code.

There was almost exact agreement of the results.

15. To further reduce the computational time required and to allow a greater area to be covered, a 1/3° by 1/3° grid was used instead of the 1/3° by 1/5° grid used in Reference 1. The validity of using the coarser grid to propagate tsunamis over the open ocean has been demonstrated.[13] Use of the latest bathymetric information for the Pacific coast of the United States allows significant improvement in the detailing of the coastline and continental shelf area.

16. The depths for the open ocean portion of the numerical grid were interpolated from data of ocean depths averaged over areas of 1° squares of latitude and longitude[14] available from the National Oceanographic Data Center. Normally, the numerical code interpolates depth data from one point per square degree to nine points per square degree. However, for the continental shelf area, the interpolation process was not used; instead, data taken directly from bathymetric charts in a form compatible with the numerical code were inserted.

17. By the modifications made to the finite difference form of the equations used in the numerical code and the use of coarser depth grid, the computational time for similar problems is reduced by a factor of approximately three as compared with the previous code.

PART V: PROCEDURE

18. To locate the hypothetical uplifts, the Peru-Chile Trench was divided into 12 equal segments as shown in Figure 3. An uplift of the same configuration as used in Reference 1 was centered in segments 1, 8, and 12. Segment 1, although closest to the Pacific coast of the continental United States, is least favorably oriented for producing large waves which propagate in that direction. Segment 8, although more favorably oriented for production of large waves, would be the segment most influenced by the "shadowing" effect of the reach of coast immediately northward of the perimeter of the uplift area. In principle, an uplift centered in segment 7 would experience more shadowing effect; but the uplift placed there would have had a significant proportion on land and therefore produce a smaller tsunami. The orientation of segment 12 is very similar to that of segment 8, i.e., more favorably oriented than segment 1 for production of large waves in the direction of the United States but without the shadowing effect experienced by segment 8. One would therefore expect the overall amplitudes of the tsunamis arriving at the Pacific coast of the United States to be least for those produced by the uplift centered in segment 8 (excluding segment 7), with tsunamis originating in the remaining eight segments producing values between those of segments 1 and 12.

19. To compare the amplitude of the leading wave of the tsunami generated by the three hypothetical ground motions as a function of distance along the Pacific coast of the United States, the amplitudes were normalized to a depth of 600 ft. This is done by analytically solving a one-dimensional standing wave equation.[15] Although other methods for calculating changes in wave amplitude due to changes in water depth have subsequently been developed (e.g., numerical algorithms based on the Korteweg-deVries equations), it is unnecessary to employ them here. In general, for a wave, the quantity $(d/L)^2$ is a measure of the dispersion while (η/d) is indicative of the degree of nonlinearity. For a tsunami at a depth of 600 ft, $(d/L)^2 \ll 1$ and $(\eta/d) \ll 1$, indicating both dispersive and nonlinear effects to be small. The ratio of the

quantities $\left[\eta/L\ (L/d)^3\right]$ is termed the Ursell number, U, and for tsunamis it can be shown that $U >> 1$, thereby making the use of Korteweg-deVries or Boussinesq equation unnecessary. The standing wave methodology is discussed in detail in Reference 1 but will be recounted briefly here.

20. Combining the one-dimensional long-wave equation of motion and the continuity equation (in rectangular coordinates) yields the wave equation

$$\frac{\partial^2 \eta(x)}{\partial t^2} = g \frac{\partial}{\partial x} d \frac{\partial \eta(x)}{\partial x} \tag{7}$$

Under the assumption of simple harmonic motion,

$$\eta \propto \cos(\omega t + \varepsilon) \tag{8}$$

and Equation 7 becomes

$$g \frac{\partial}{\partial x} \frac{\partial \eta(x)}{\partial x} + \omega^2 \eta(x) = 0 \tag{9}$$

Substituting $d(x) = d_a x/a$ and $k = \omega^2 a/g d_a$ where d_a is the water depth at the gage location some distance $x = a$ from the shoreline in Equation 9 gives,

$$\frac{\partial}{\partial x} x \frac{\partial \eta(x)}{\partial x} + k\eta(x) = 0 \tag{10}$$

The solution to Equation 10 is

$$\eta(x) = AJ_o(2k^{1/2}x^{1/2}) \tag{11}$$

or with the time dependence restored

$$\eta(x,t) = AJ_o(2k^{1/2}x^{1/2}) \cos(\omega t + \varepsilon) \tag{12}$$

Because a tsunami has a very long wavelength, it can be assumed that

the entire local water surface oscillates in the vicinity of some local depth, d, where $x \geq a$, thus

$$\eta(x) = C \cos(\omega t + \varepsilon) \tag{13}$$

for $x \geq a$. Equating Equations 12 and 13 yields

$$A = \frac{C}{J_o(2k^{1/2}a^{1/2})} \tag{14}$$

Therefore,

$$\eta(x) = C \frac{J_o(2k^{1/2}x^{1/2})}{J_o(2k^{1/2}a^{1/2})} \cos(\omega t + \varepsilon) \tag{15}$$

Solving for C at $x = a$

$$C = \frac{\eta(a)}{\cos(\omega t + \varepsilon)} \tag{16}$$

From Equation 15

$$\eta(b) = C \frac{J_o(2k^{1/2}b^{1/2})}{J_o(2k^{1/2}a^{1/2})} \cos(\omega t + \varepsilon) \tag{17}$$

and substituting Equation 16

$$\eta(b) = \frac{J_o(2k^{1/2}b^{1/2})}{J_o(2k^{1/2}a^{1/2})} \eta(a) \tag{18}$$

Since $\eta(a)$ is known from the numerical simulation, η at $x = b$ can be determined. The values of a, b, and d_a are determined from National Ocean Survey charts.

21. Because the method described above is one-dimensional, it accounts for the effects of shoaling and reflection but not refraction or diffraction. However, since a tsunami wavelength is so great in waters deeper than 600 ft, few bathymetric features are large enough to significantly refract or diffract the waves over relatively short distance from the nearest gage location to the 600-ft contour.

PART VI: RESULTS

22. Table 2 shows a comparison of amplitudes of the leading wave of the 1960 Chilean tsunami as recorded by tide gages at selected exposed locations with results of the numerical simulation at locations nearest the tide gages. To avoid the false appearance of exact agreement at locations such as Port Hueneme, the results of the numerical simulation are rounded to the nearest hundredth foot rather than the nearest tenth. It is quite proper to compare the leading wave of the actual tsunami with the leading wave of the simulation since, for large tsunamis with minimal frequency dispersion, the leading wave will practically always be the largest wave in water depths where the comparisons are made (approximately 600 ft or more at the edge of the continental shelf). In cases where subsequent waves (at the shoreline) are larger than the initial wave, it is almost always due to shelf and bay resonance which occurs shoreward of the point where the comparisons are being made.

23. Ideally, the amplitudes resulting from the simulation should be slightly less than those recorded at corresponding tide gages because of shoaling of the wave into shallower gage locations. With the exception of the Presidio gage, this is indeed the case. Two factors which could account for the anomaly at Presidio are: (a) frictional dissipation of the actual tsunami over the broad, shallow shelf seaward of Presidio which is not considered in the governing equations of the code, and (b) the averaged discretized depths in the finite difference program cover too large an area to represent the detail of the shelf accurately.

24. Figures 5-19 show contours of sea surface elevation of the leading tsunami waves generated by simulation of the 1960 Chilean quake and by hypothetical uplifts centered in segments 1, 8, and 12 at times specified in the figures. The reason for the extensive damage caused by the 1960 Chilean tsunami in the Hawaiian Islands and Japan is evident as the highest section of the wave front is directed toward these locations (Figures 7 and 8). The directivity of the three hypothetical uplifts is also evidenced in their respective figures, with uplifts in segments 1 and 12 radiating the largest waves primarily northwestward

and segment 8 radiating its largest primarily westward. The preferential radiational patterns of noncircular uplifts is well documented.[16,17]

25. Figure 20 shows the locations of the 64 gages used to determine the leading wave amplitude as a function of distance along the Pacific coast of the United States. Figures 21-23 are plots of the amplitude of the leading wave of tsunamis generated by hypothetical uplifts located in segments 1, 8, and 12, respectively. While tsunamis generated in segments 1 and 12 generally produce similar responses along the Pacific coast, the response to the tsunami generated in segment 8 is markedly less. This is probably due to the shadowing by the northwestward to southeastward oriented stretch of South American coast between lat. 15 and 20° S. The generally low response exhibited along the coast from about San Diego to Los Angeles due to tsunamis generated in the three segments is probably the result of sheltering by the Channel Islands. The peaks shown in the vicinity of Port Hueneme (1.4 to 3.3 ft) agree fairly well with heights recorded there during past tsunamis, e.g., 1960 Chilean, 2 ft; 1957 Aleutian, <3.5 ft. The validity of the large peaks shown in Figures 21 and 23 just south of Pt. Sur is unknown. No gage records exist near that location with which to compare results; also, it is a relatively uninhabited stretch of coastline. The response of the remainder of coastline is relatively uniform with a maximum amplitude variation of about 1.5 ft. This is not unexpected due to the gradual eastward turning of the coastline as one proceeds northward.

PART VII: SUMMARY

26. The Peru-Chile Trench has a long recorded history as an area of generation of tsunamis that cause significant runup along the Pacific coast of the continental United States. An explicit numerical code has been developed and is demonstrated to adequately hindcast the Chilean tsunami of 22 May 1960. The code is used to simulate the generation and propagation of tsunamis with intensities approximately equal to four which originate in the Peru-Chile Trench. The amplitudes of the tsunamis are normalized to 600-ft depth and are plotted as a function of distance along the U. S. west coast from the Mexican to the Canadian Borders, thus allowing a relative comparison of the vulnerability of various locations along the U. S. west coast to tsunamis originating in the Peru-Chile Trench.

27. Because of priorities within the Civil Works R&D program, funding for Work Unit No. 31093 was terminated with completion of the work reported herein. If and when funding of this Work Unit is resumed, the logical next steps would consist of (a) designating the locations of existing and potential harbor sites on the Pacific coast, (b) propagating tsunami waves into each harbor site from probable tsunami sources to determine the potential for damage, and (c) exploring the alternatives of relocating proposed harbor sites, providing adequate structural protection, or modifying the hydrography of the areas in such manner that tsunami waves would be attenuated to the point that major damage would be prevented. These additional steps are necessary to meet the objectives of this Work Unit.

REFERENCES

1. Houston, J. R. et al., "Effect of Source Orientation and Location in the Aleutian Trench on Tsunami Amplitude Along the Pacific Coast of the Continental United States," Research Report H-75-4, Jul 1975, U. S. Army Engineer Waterways Experiment Station, CE, Vicksburg, Miss.

2. Kelleher, J. et al., "Why and Where Great Thrust Earthquakes Occur Along Island Arcs," Journal, Geophysical Research, Vol 79, No. 32, 1974, pp 4889-4899.

3. Kelleher, J. A., "Rupture Zones of Large South American Earthquakes and Some Predictions," Journal, Geophysical Research, Vol 77, No. 11, 1972, pp 2087-2103.

4. Sykes, L. R., "Aftershock Zones of Great Earthquakes, Seismicity Gaps and Earthquake Prediction of Alaska and the Aleutians," Journal, Geophysical Research, Vol 76, No. 32, 1971, pp 8021-8041.

5. Lomnitz, C., "Major Earthquakes and Tsunamis in Chile During the Period 1535-1955," Geologische Rundschau, Band 59, Heft 3, 1970, pp 938-960.

6. Symons, J. M. and Zetler, B. D., "The Tsunami of May 22, 1960 as Recorded at Tide Stations," Preliminary Report, U. S. Department of Commerce, Coast and Geodetic Survey, Washington, D. C.

7. Chinnery, M. A. and North, R. G., "The Frequency of Very Large Earthquakes," Science, Vol 190, No. 4219, 1975.

8. Hayes, D. E. "Geophysical Investigation of the Peru-Chile Trench," Marine Geology, Vol 4, 1966, pp 309-351.

9. Plafker, G. and Savage, J. C., "Mechanism of the Chilean Earthquakes of May 21 and 22, 1960," Bulletin, Geological Society of America, Vol 81, No. 4, pp 1001-1030, 1970.

10. Hwang, L.-S., Divoky, D., and Yuen, A., "Amchitka Tsunami Study," Report TC-177, 1970, Tetra-Tech, Inc., Pasadena, Calif.

11. Houston, J. R. and Garcia, A. W., "Type 16 Flood Insurance Study: Tsunami Predictions for Pacific Coastal Communities," Technical Report H-74-3, May 1974, U. S. Army Engineer Waterways Experiment Station, CE, Vicksburg, Miss.

12. Garcia, A. W. and Houston, J. R., "Type 16 Flood Insurance Study: Tsunami Predictions for Monterey and San Francisco Bays and Puget Sound," Tehcnical Report H-75-17, Nov 1975, U. S. Army Engineer Waterways Experiment Station, CE, Vicksburg, Miss.

13. Houston, J. R. et al., "Probable Maximum Tsunami Runup for Distant Seismic Events - Islote Site, Puerto Rico," Amendment 23, NORCO-NP-1 PSAR, May 1975, Puerto Rico Water Resources Authority, Fugro, Inc.

14. Smith, S. M., Menard, H. W., and Sharman, G., "World-Wide Ocean Depths and Continental Elevations Averaged for Areas Approximating One Degree Squares of Latitude and Longitude," Mar 1966, Scripps Institution of Oceanography, LaJolla, Calif.

15. Lamb, H., Hydrodynamics, 6th ed., Cambridge University Press, New York, 1932.

16. Takahashi, R. and Hatori, T., "A Model Experiment on the Tsunami Generation from a Bottom Deformation Area of Elliptic Shape," Bulletin, Earthquake Research Institute, Vol 40, 1962, pp 873-883.

17. Hatori, T., "Directivity of Tsunamis," Bulletin, Earthquake Research Institute, Vol 41, 1963, pp 61-81.

Table 1

Maximum Recorded Rise or Fall of Wave Heights

Station	Wave Height, ft, for Year				
	1946	1952	1957	1960	1964
Honolulu, Hawaii	4.1	4.4	3.2+*	5.5+*	2.7
Sitka, Alaska	2.6	1.5	2.6	3.0	14.3
Neah Bay, Wash.	1.2	1.5	1.0	2.4	4.7
Crescent City, Calif.	5.9	6.8	4.3	10.9	(Gage failed)
San Francisco, Calif.	1.7	3.5	1.7	2.9	7.4
Port Hueneme, Calif.	5.5	4.7	3.5	8.8	--
Los Angeles (Berth 60), Calif.	2.5	2.0	2.1	5.0	3.2
La Jolla, Calif.	1.4	0.8	2.0	3.3	2.2
San Diego, Calif.	1.2	2.3	1.5	4.6	3.7

* Measured rise or fall. No extrapolation made for height beyond gage limit.

Table 2

Comparison of Elevations of Maximum Rise of Initial Wave of 1960 Peru-Chile Tsunami to Numerical Simulation

Gage Location	1960 Peru-Chile Tsunami, ft	Numerical Simulation ft
La Jolla, Calif.	1.4	1.05
San Clemente Island, Calif.	0.9	0.89
Port Hueneme, Calif.	1.9	1.86
Presidio (San Francisco), Calif.	1.3	1.46
Crescent City, Calif.	1.3	1.02
Neah Bay, Wash.	0.9	0.73

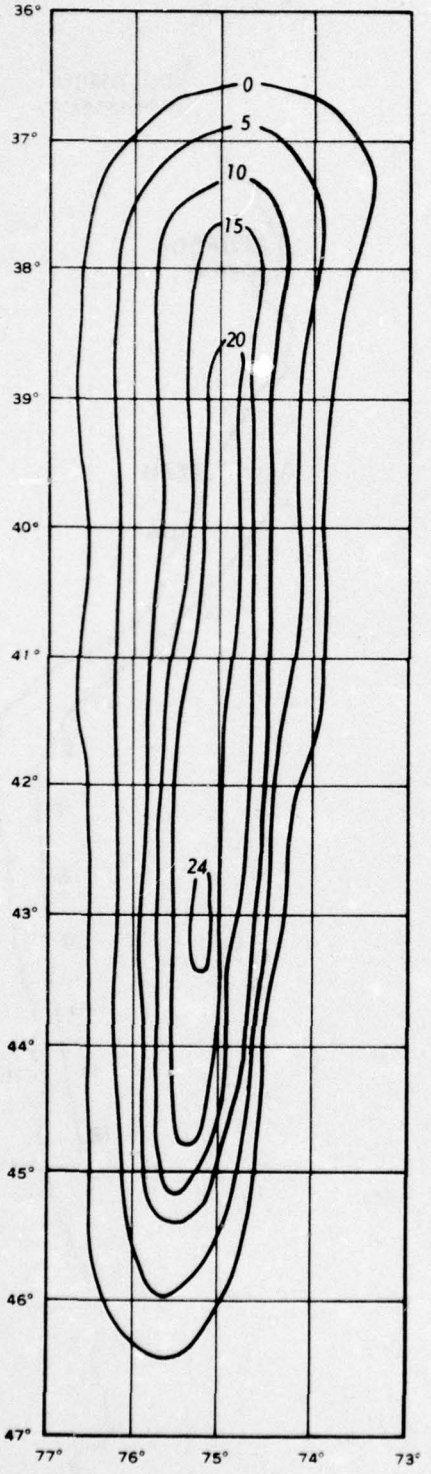

Figure 1. Contours of uplift used to simulate 1960 Chilean earthquake

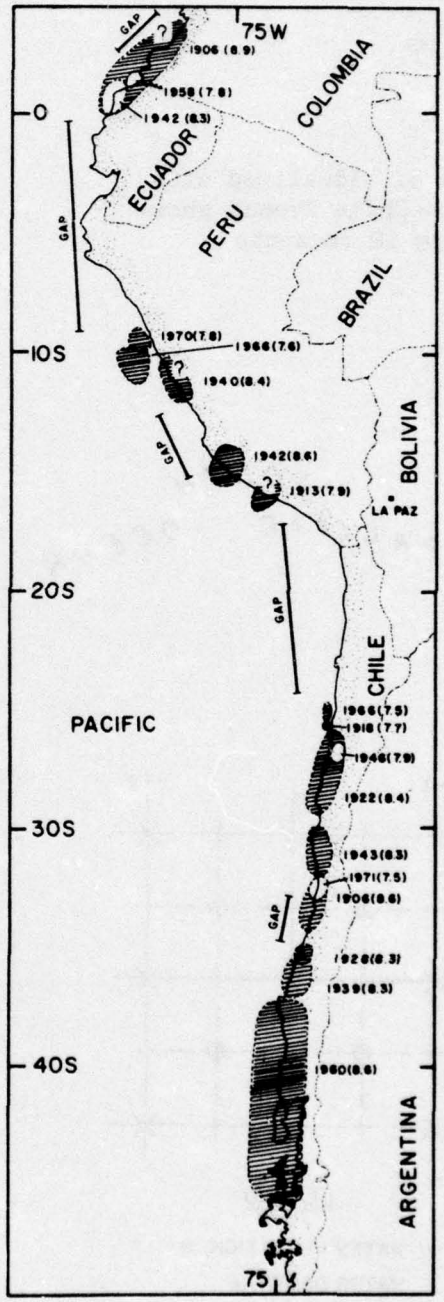

Figure 2. Rupture zones for large shallow earthquakes of this century and existing seismic gaps (after Kelleher[3])

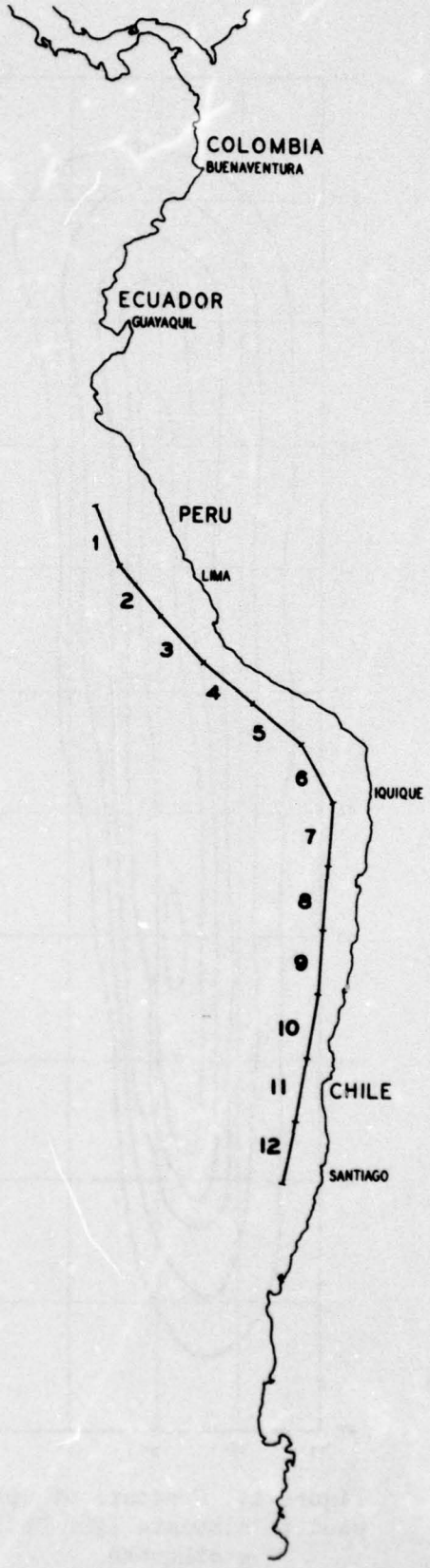

Figure 3. Idealized axis of Peru-Chile Trench showing 12 segments

SOUTH PACIFIC OCEAN

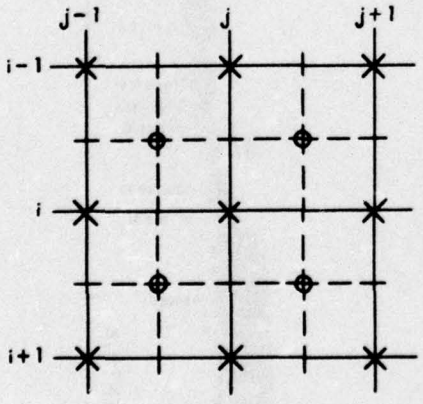

LEGEND

X – WATER ELEVATION, η

O – WATER DEPTH, d

– – U VELOCITY IN DIRECTION, θ

| – V VELOCITY IN DIRECTION, ϕ

Figure 4. Graphic representation of the finite difference grid

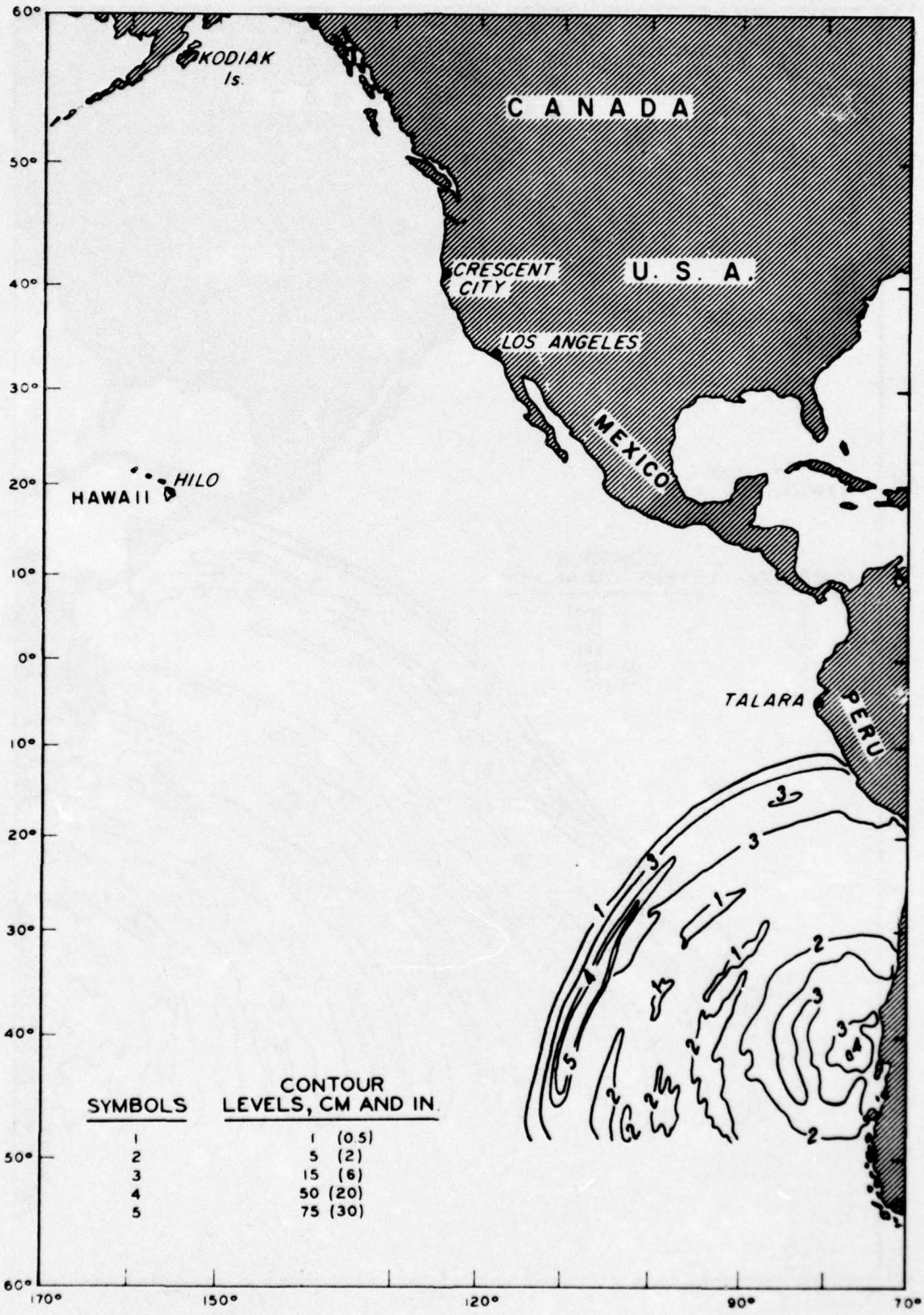

Figure 5. Contours of water-surface elevation for the leading tsunami waves 4 hr after simulation of the 1960 Chilean earthquake

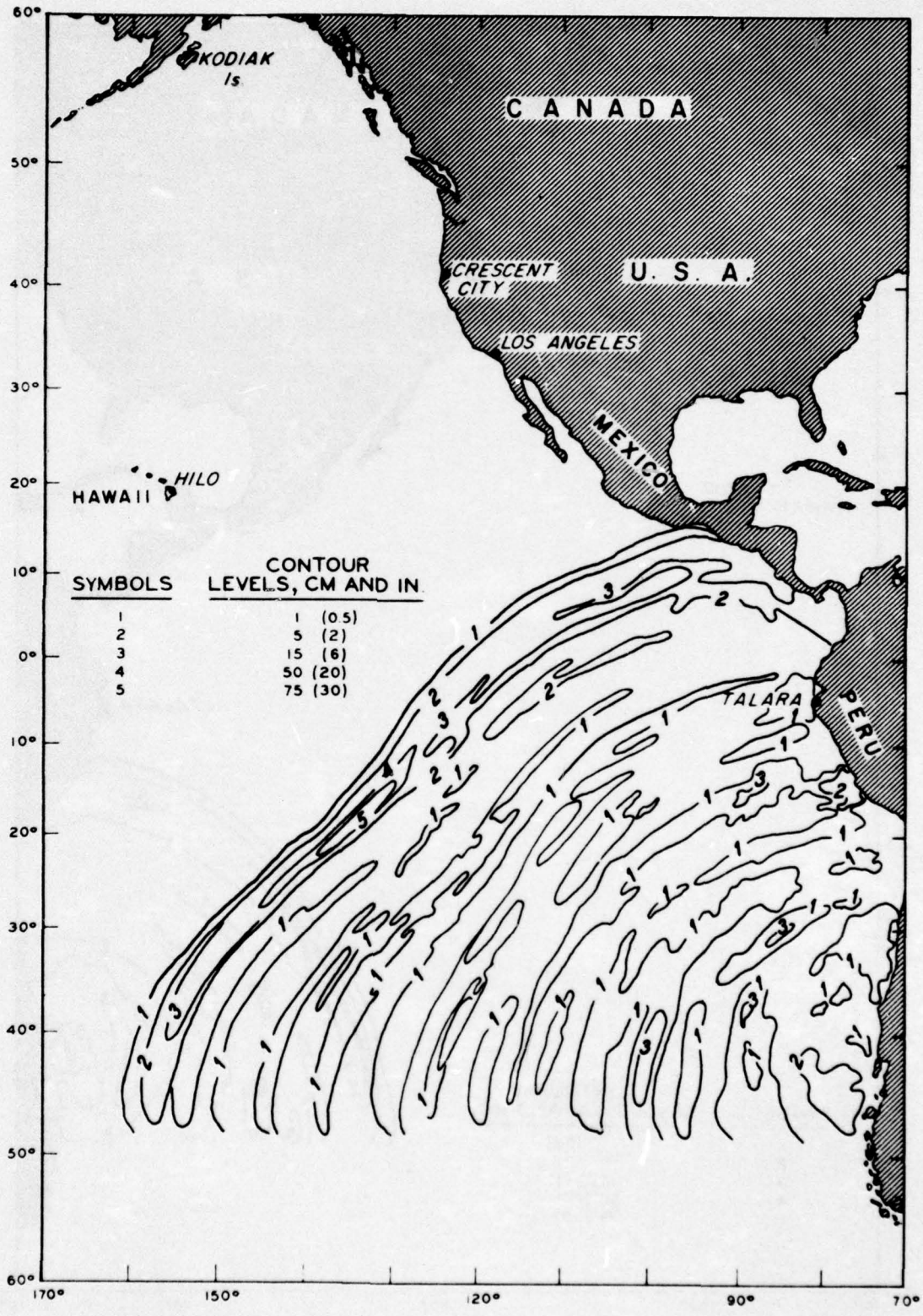

Figure 6. Contours of water-surface elevation for the leading tsunami waves 9 hr after simulation of the 1960 Chilean earthquake

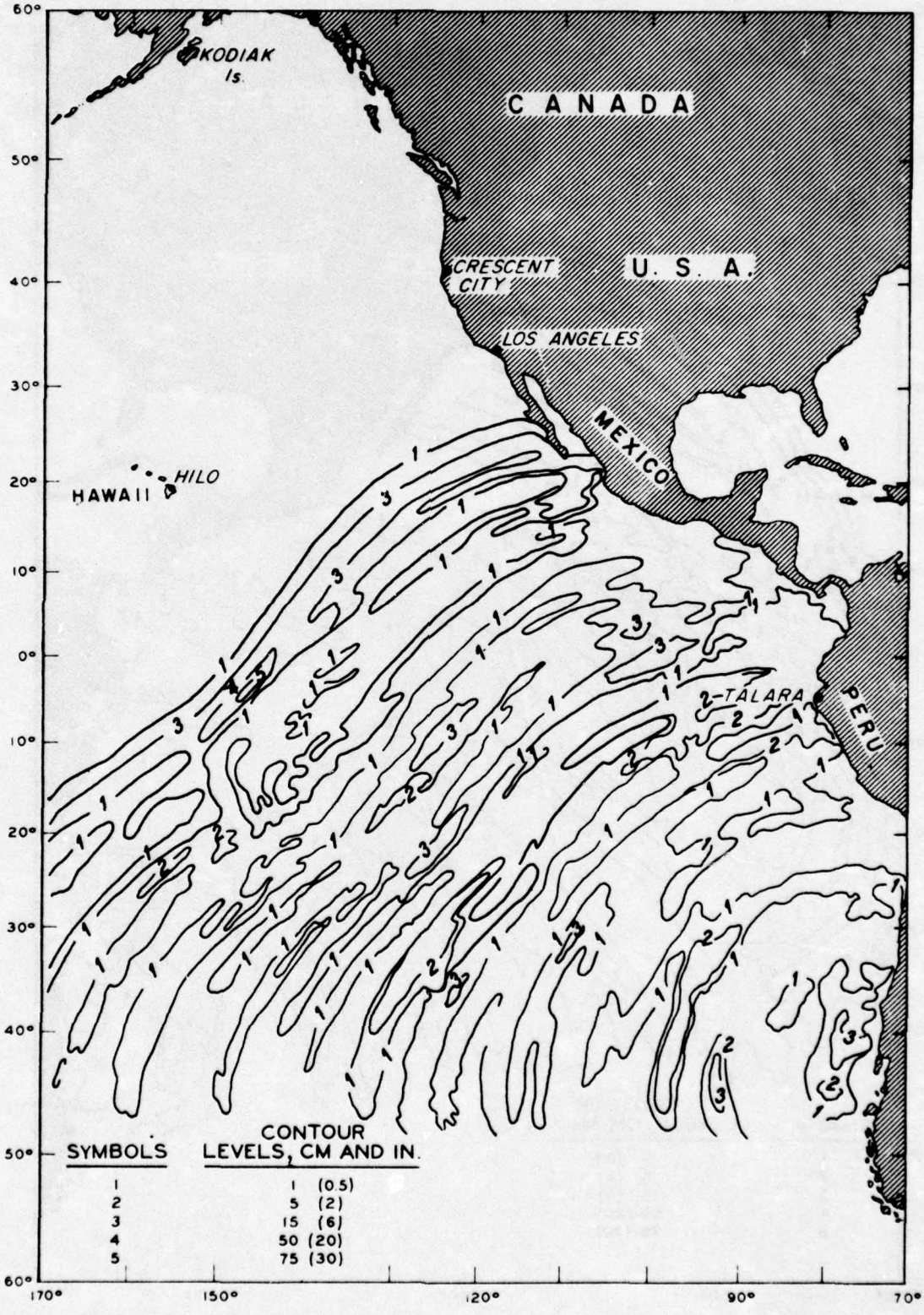

Figure 7. Contours of water-surface elevation for the leading tsunami waves 12 hr after simulation of the 1960 Chilean earthquake

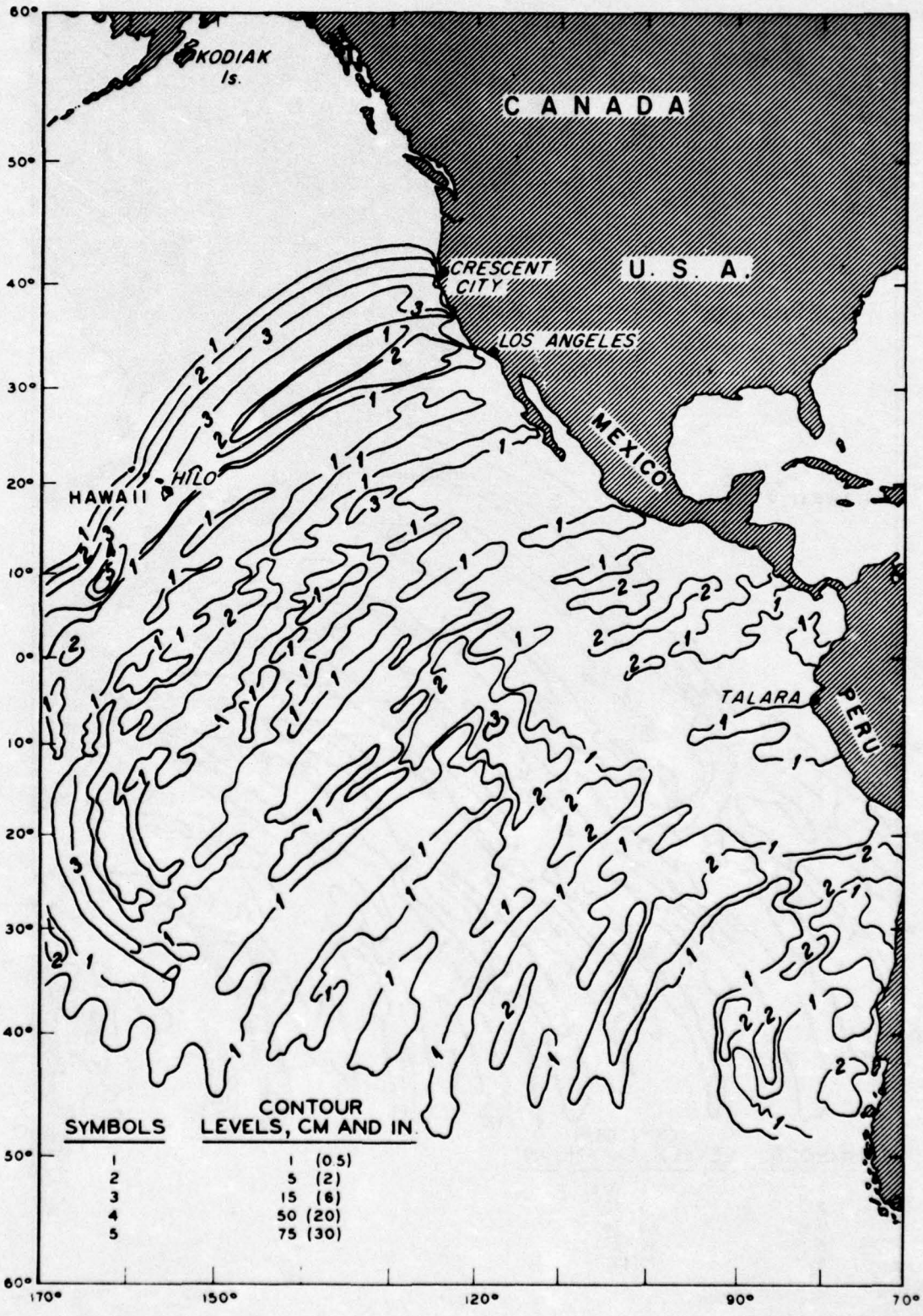

Figure 8. Contours of water-surface elevation for the leading tsunami waves 15 hr after simulation of the 1960 Chilean earthquake

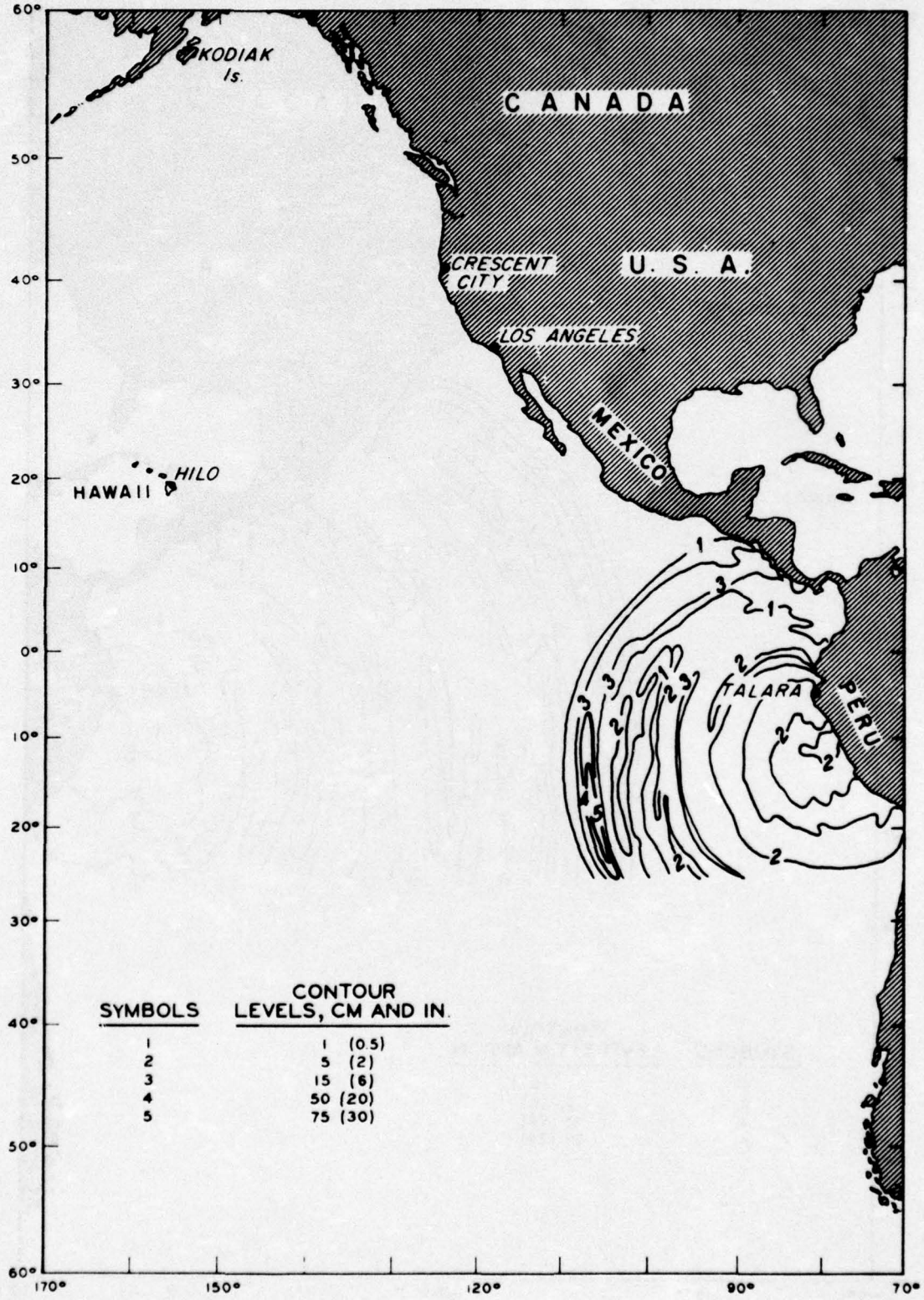

Figure 9. Contours of water-surface elevation for leading tsunami waves 4 hr after ground uplift in segment 1

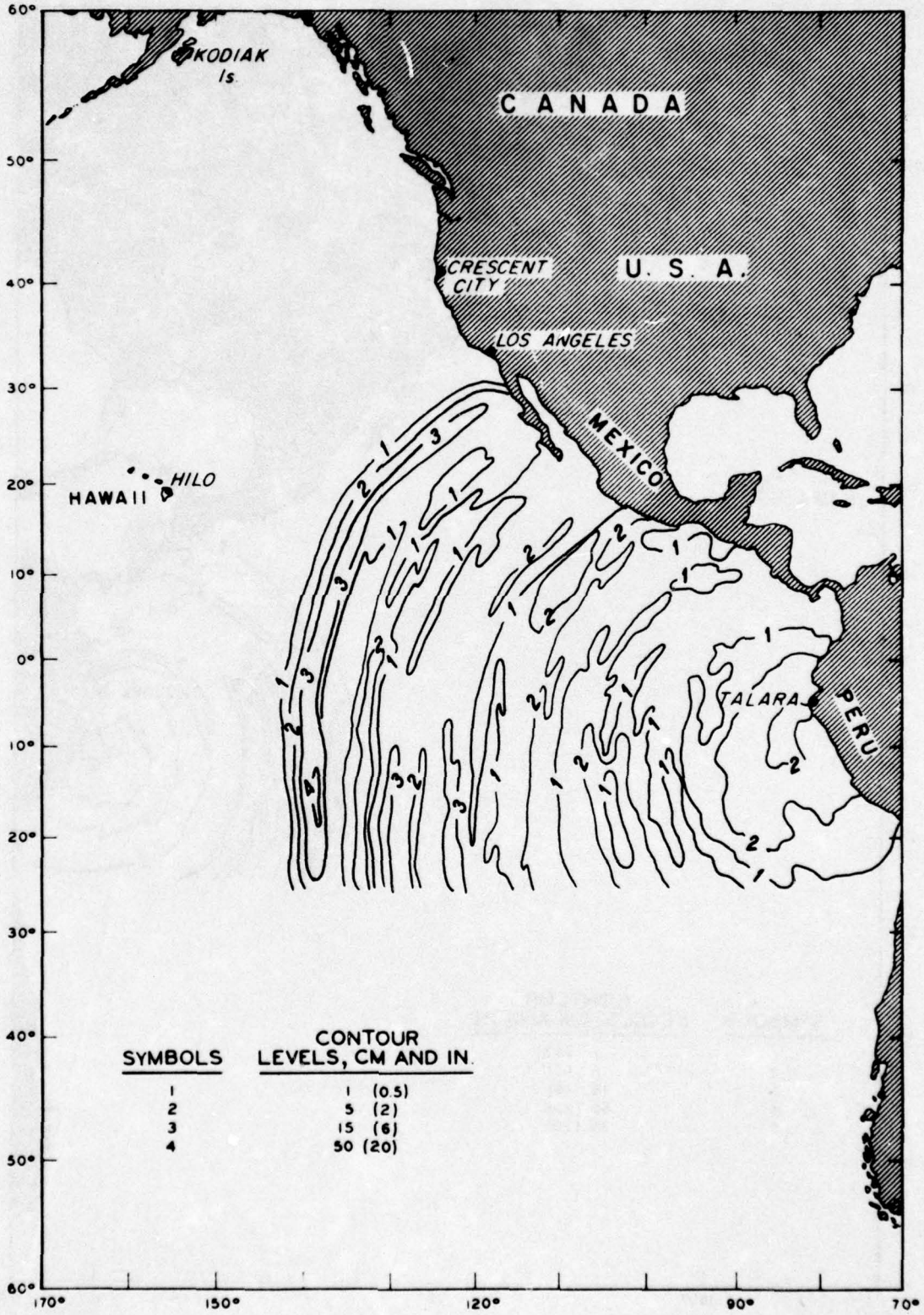

Figure 10. Contours of water-surface elevation for the leading tsunami waves 9 hr after ground uplift centered in segment 1

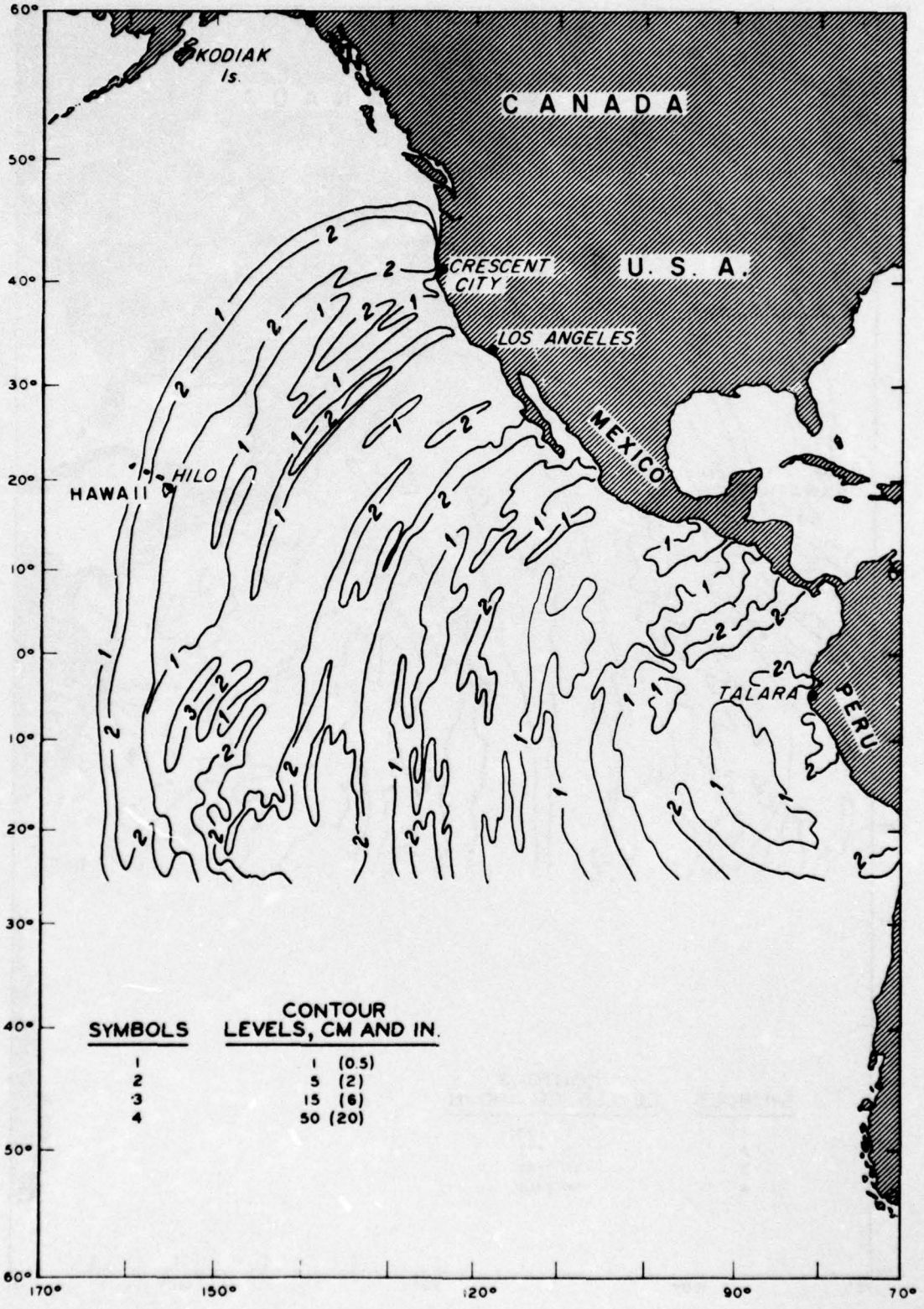

Figure 11. Contours of water-surface elevation for the leading tsunami waves 12 hr after ground uplift centered in segment 1

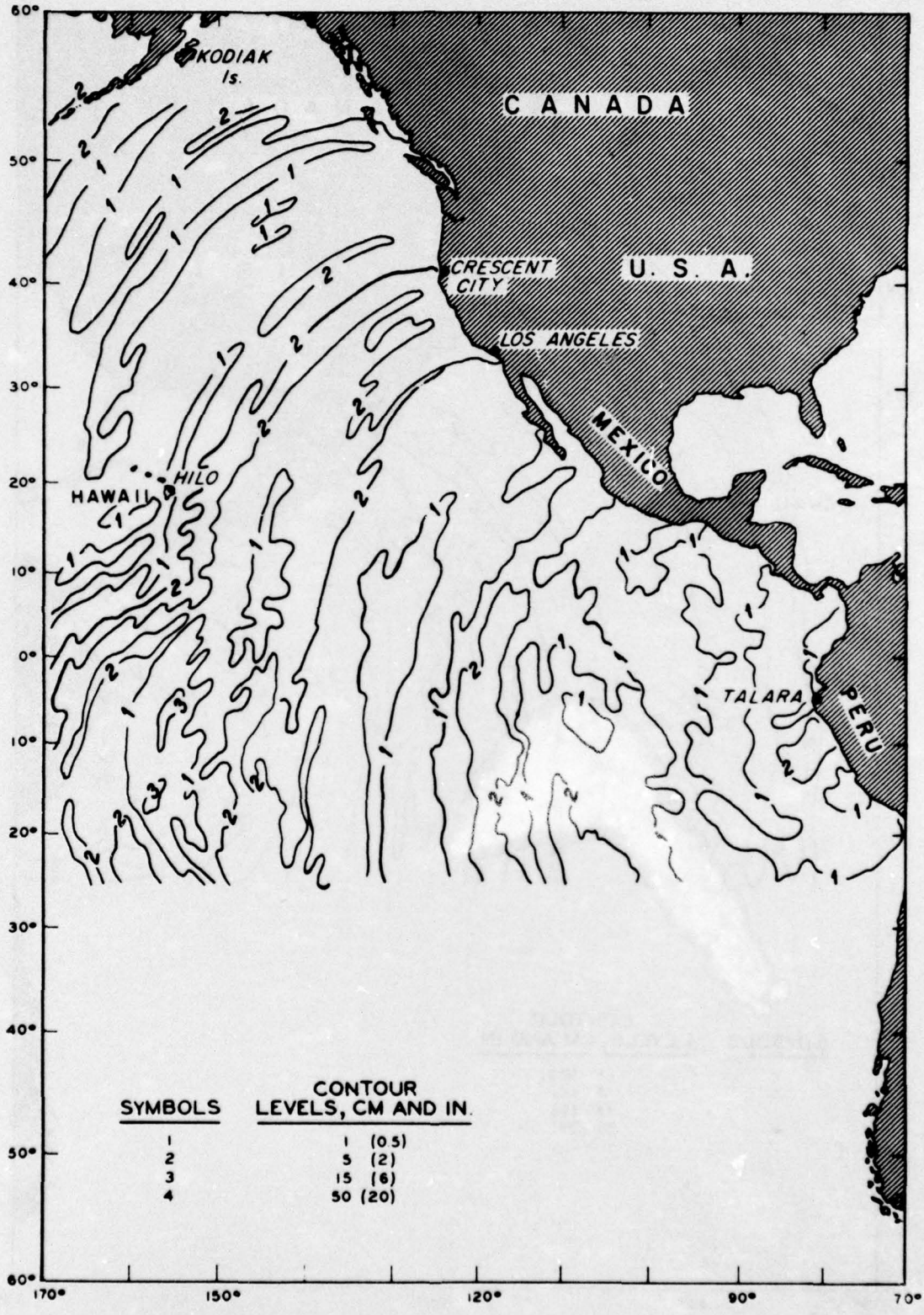

Figure 12. Contours of water-surface elevation for the leading tsunami waves 15 hr after ground uplift centered in segment 1

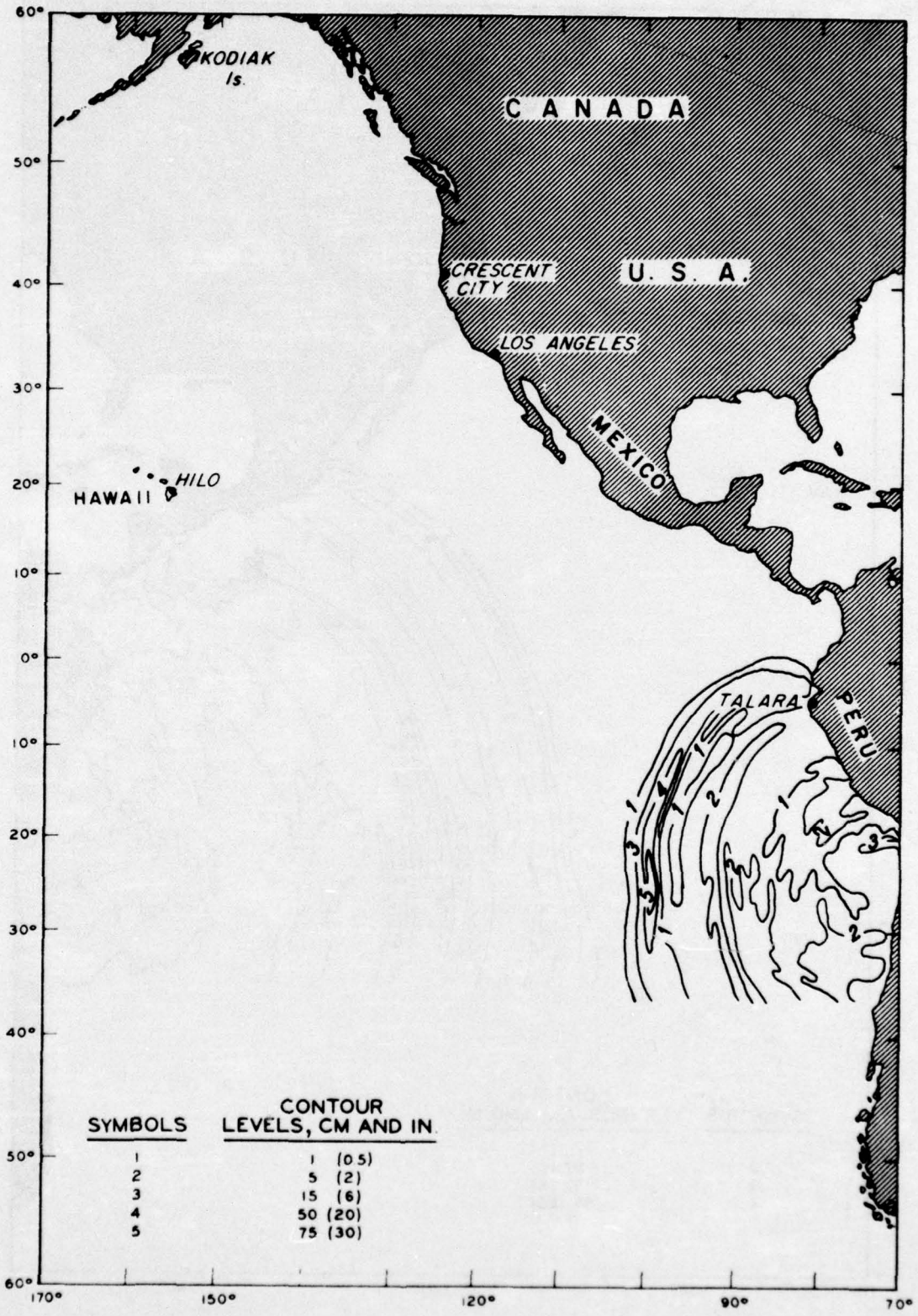

Figure 13. Contours of water-surface elevation for the leading tsunami waves 4 hr after ground uplift centered in segment 8

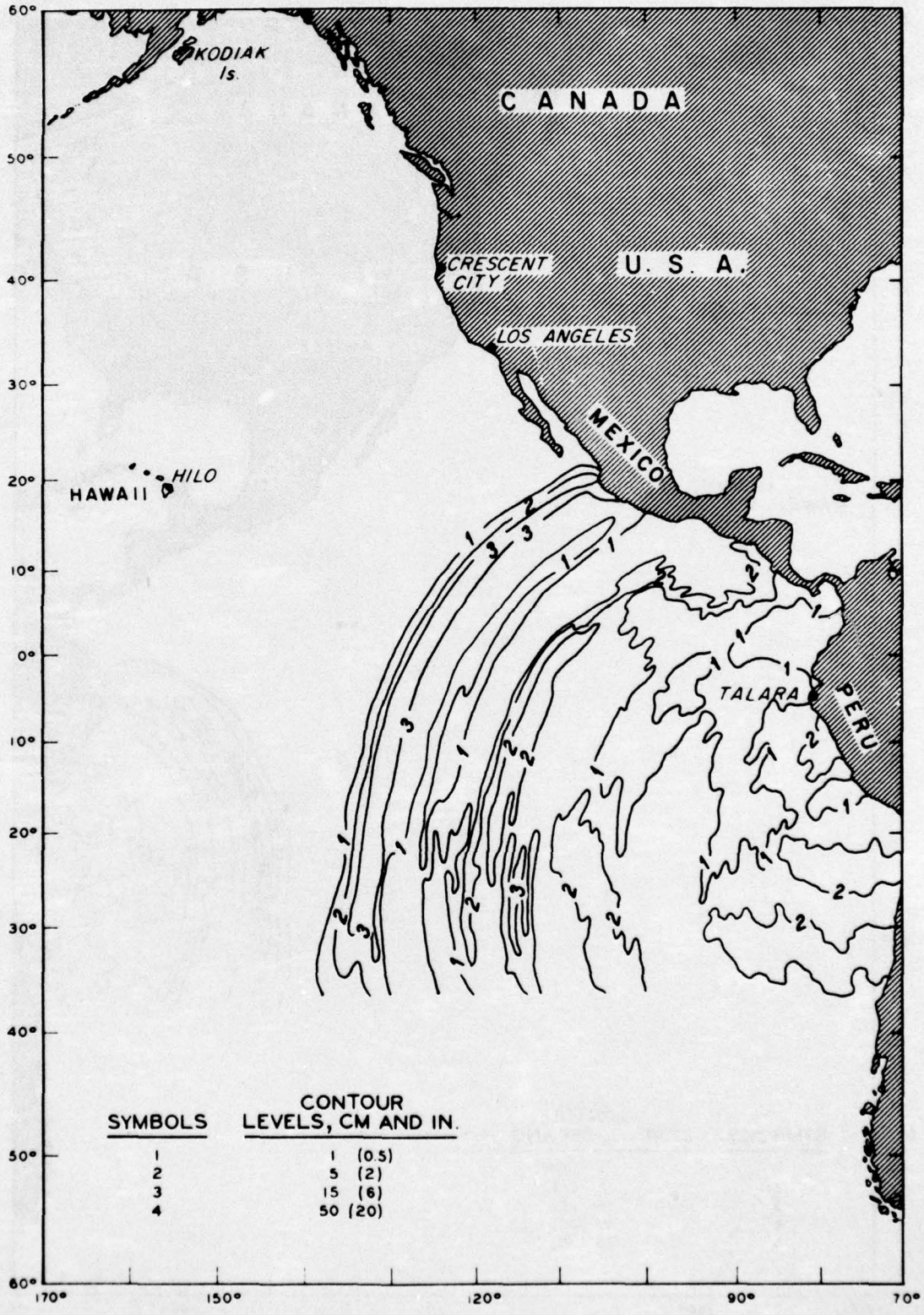

Figure 14. Contours of water-surface elevation for the leading tsunami waves 9 hr after ground uplift centered in segment 8

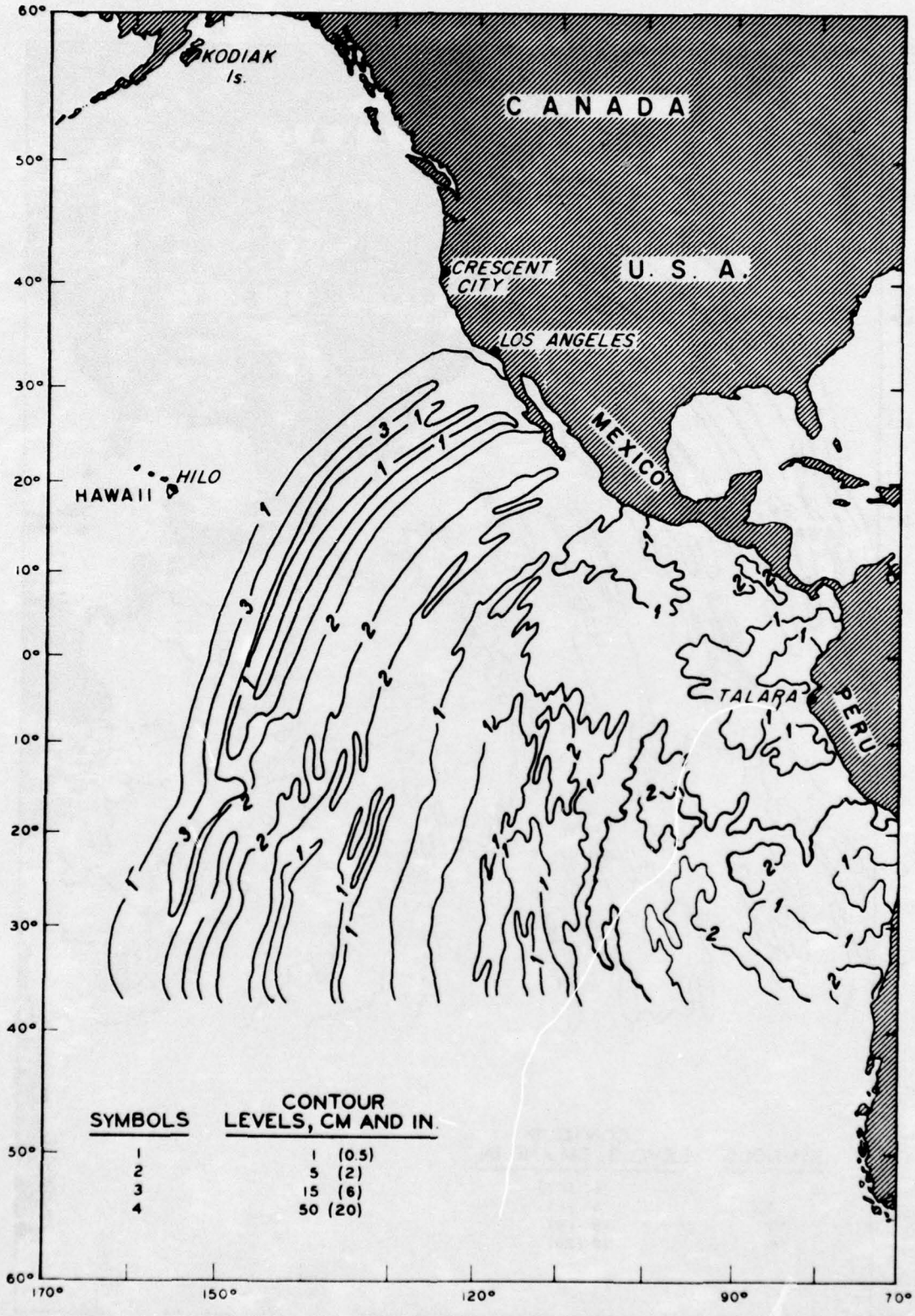

Figure 15. Contours of water-surface elevation for the leading tsunami waves 12 hr after ground uplift centered in segment 8

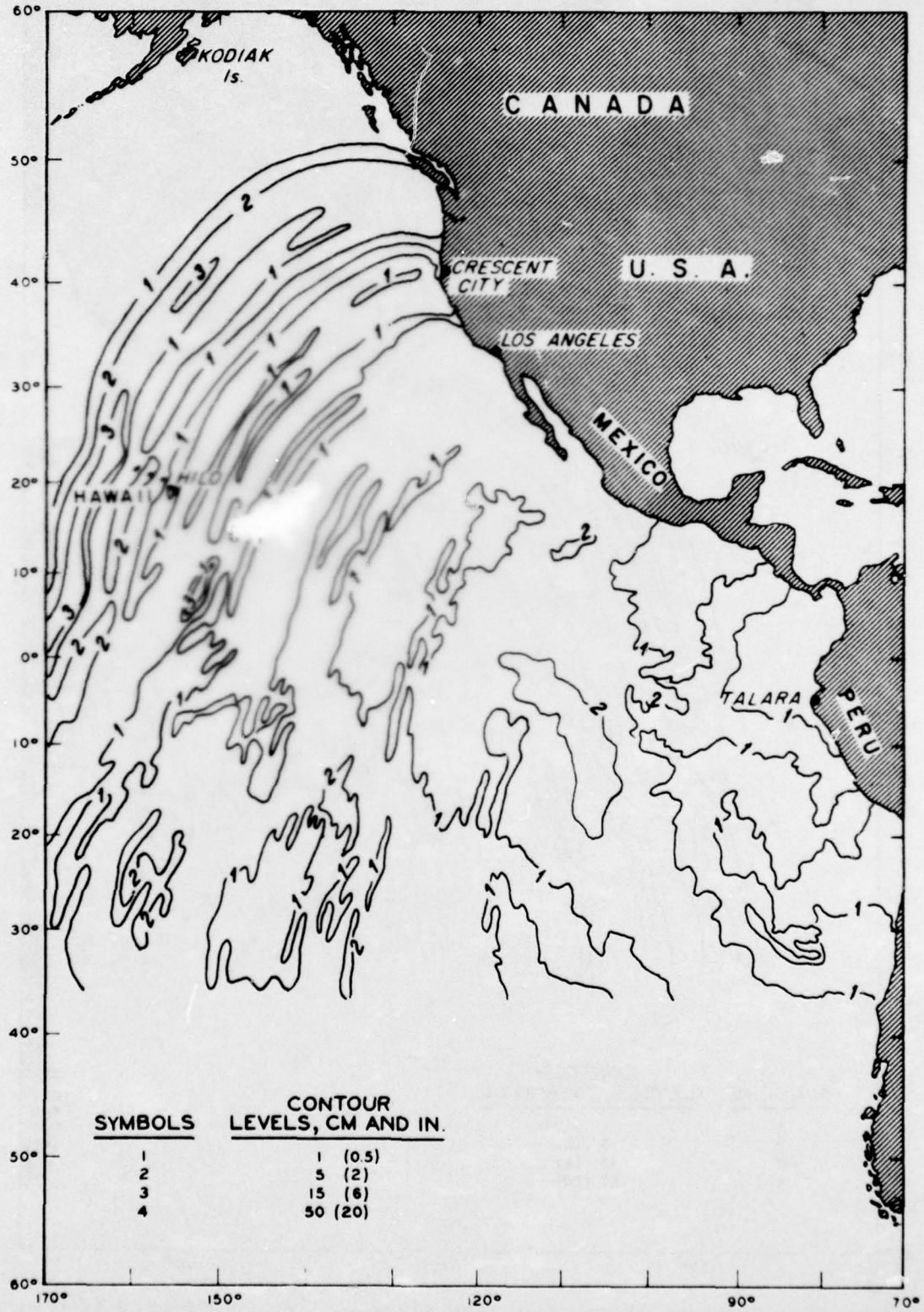

Figure 16. Contours of water-surface elevation for the leading tsunami waves 15 hr after ground uplift centered in segment 8

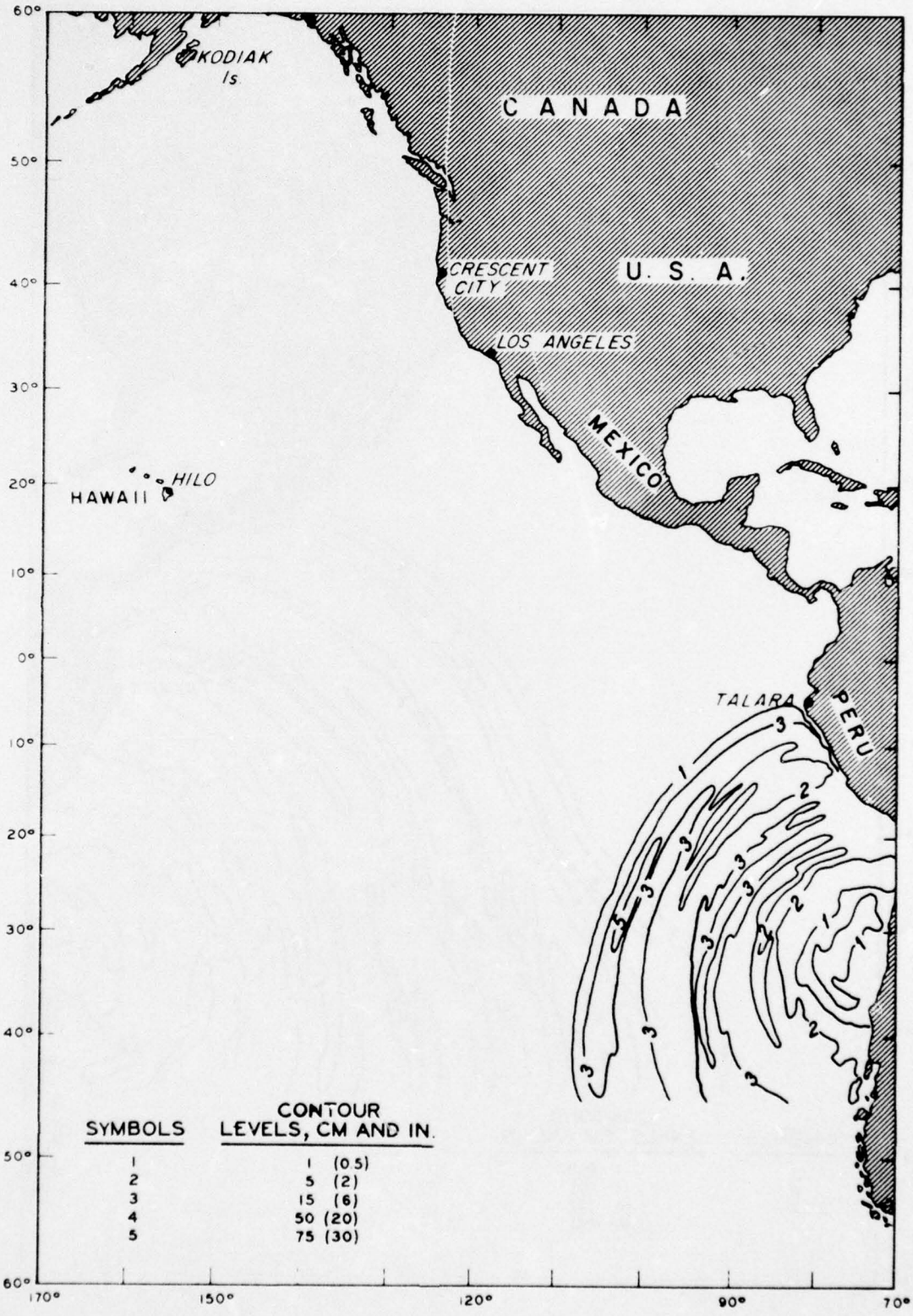

Figure 17. Contours of water-surface elevation for the leading tsunami waves 4 hr after ground uplift centered in segment 12

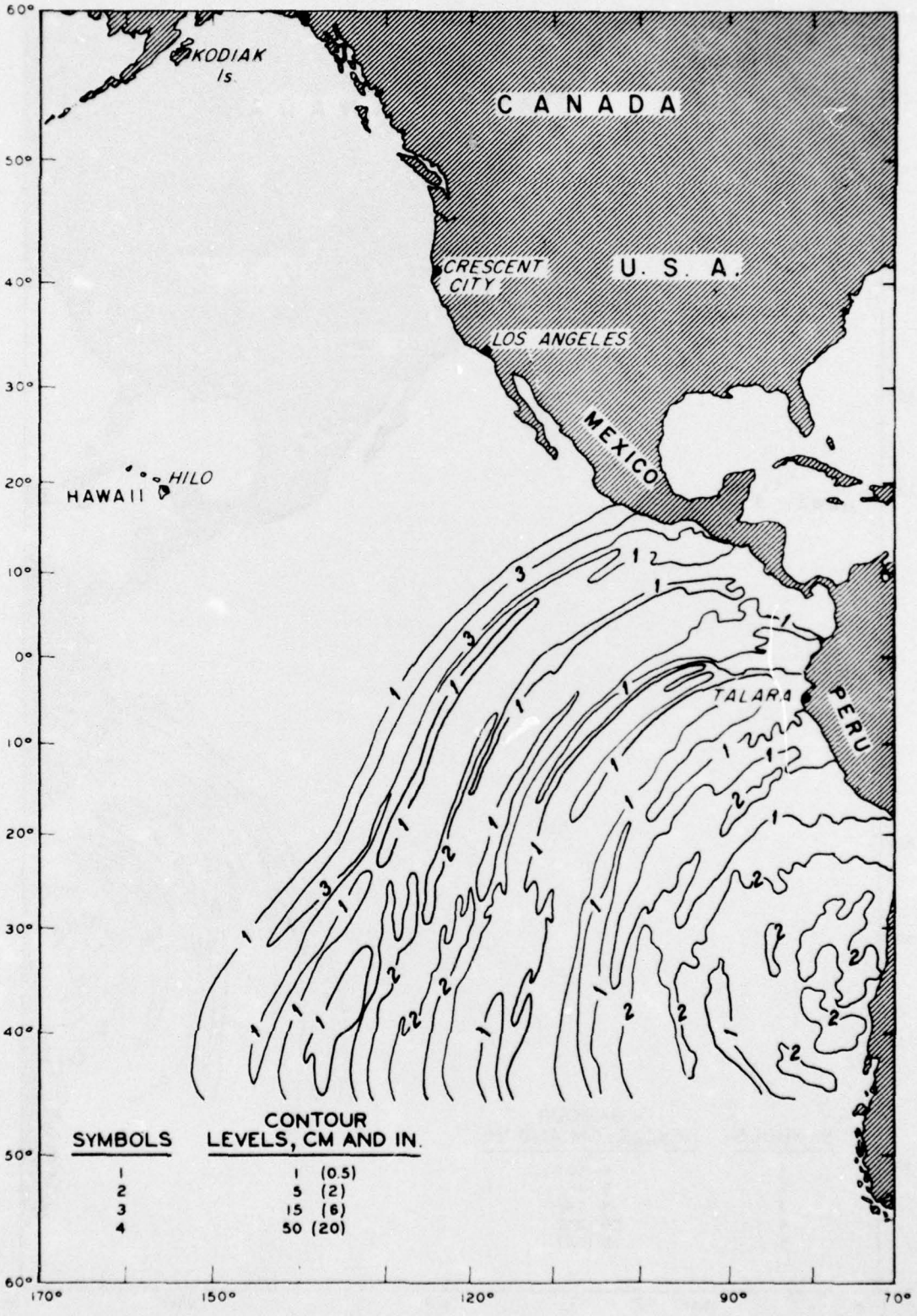

Figure 18. Contours of water-surface elevation for the leading tsunami waves 9 hr after ground uplift centered in segment 12

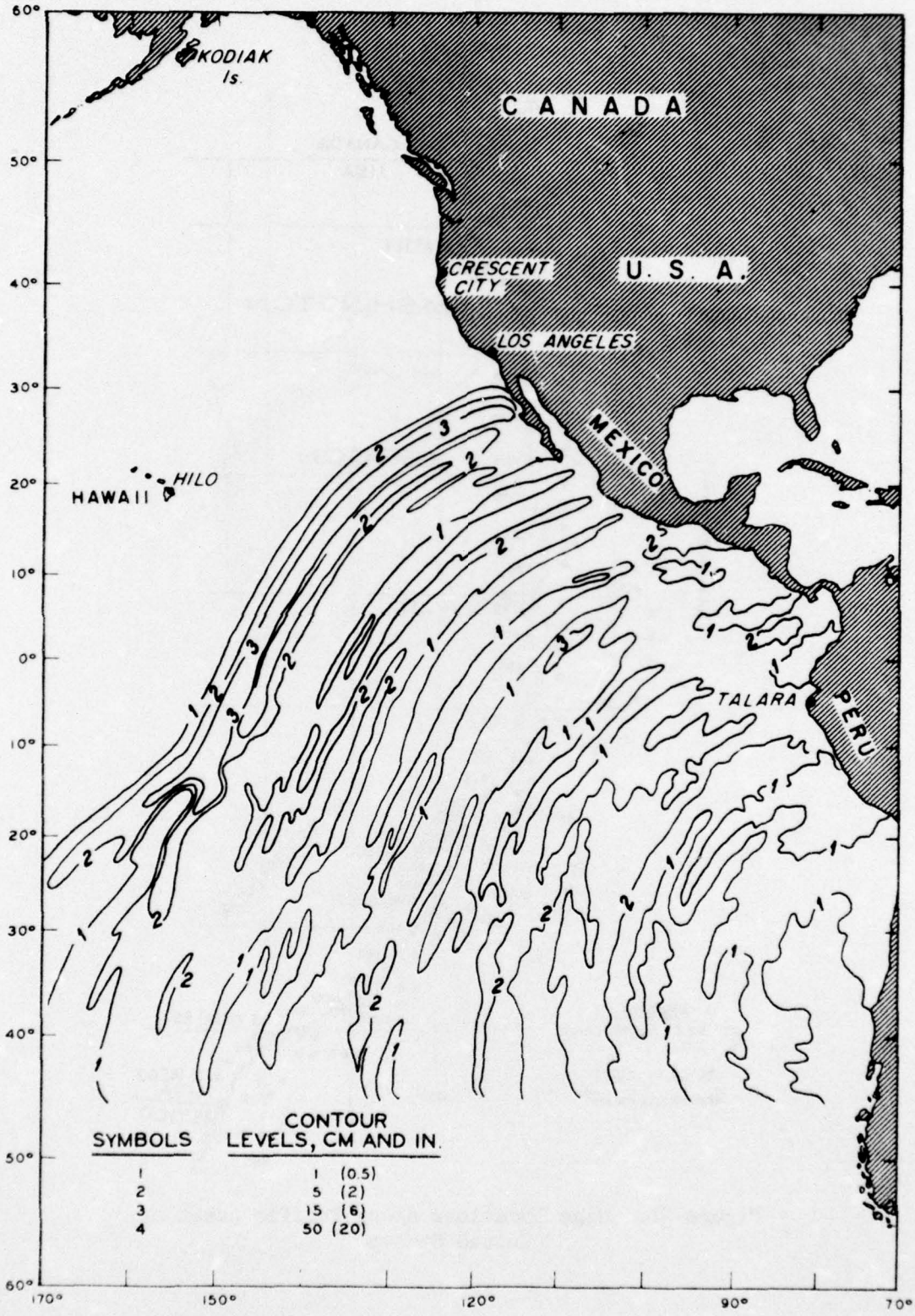

Figure 19. Contours of water-surface elevation for the leading tsunami waves 12 hr after ground uplift centered in segment 12

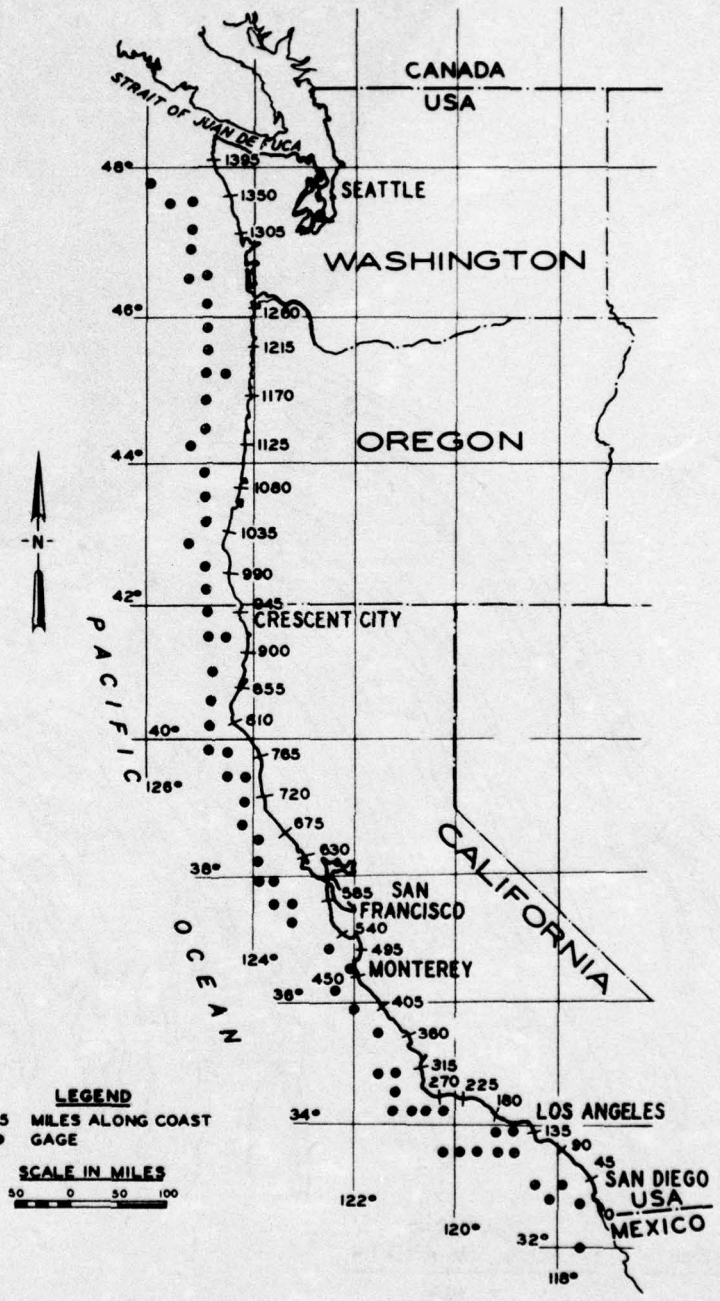

Figure 20. Gage locations along Pacific coast of United States

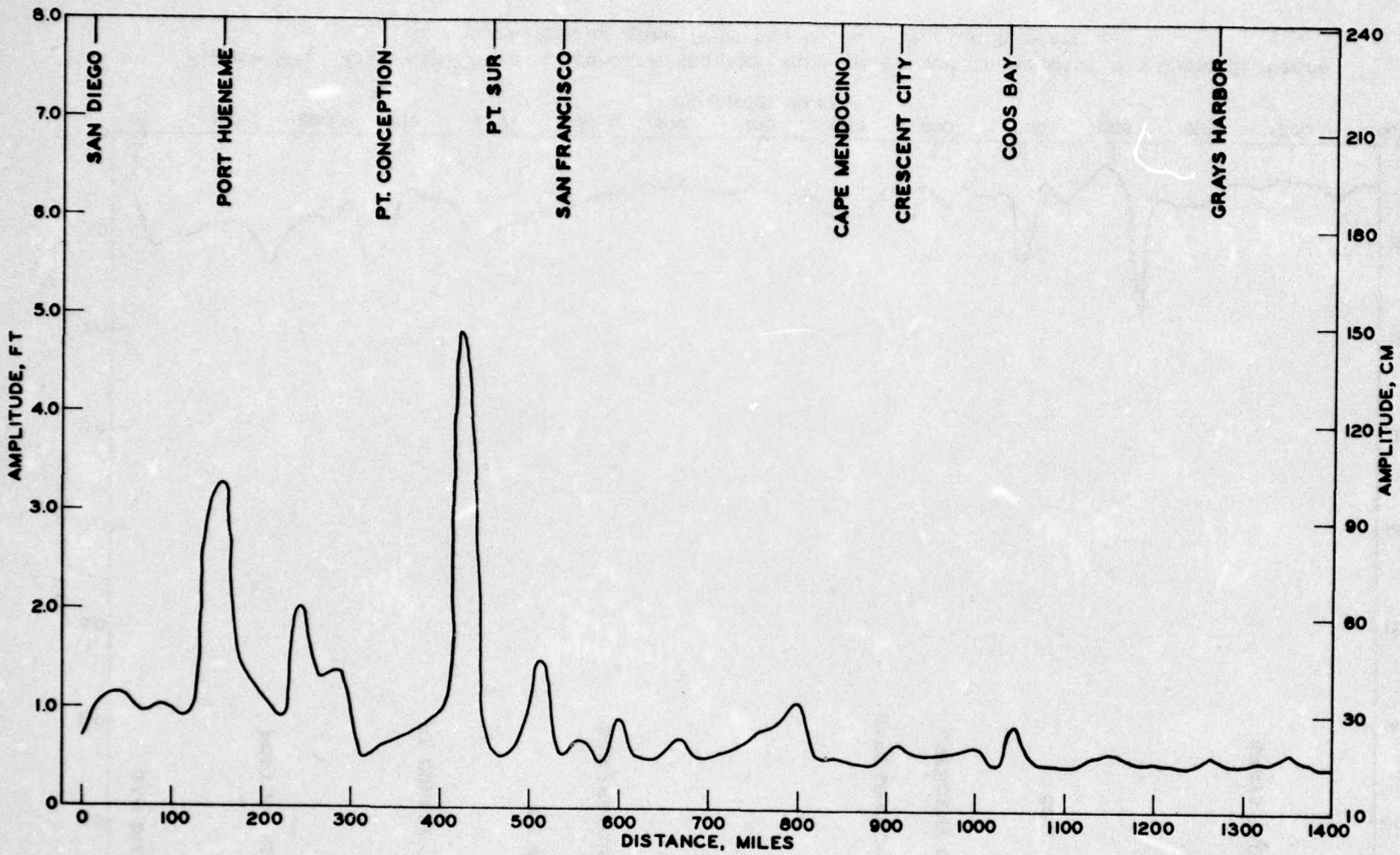

Figure 21. Wave amplitude of leading tsunami wave generated in segment 1 versus distance of the recording gage from the U. S. - Mexico border

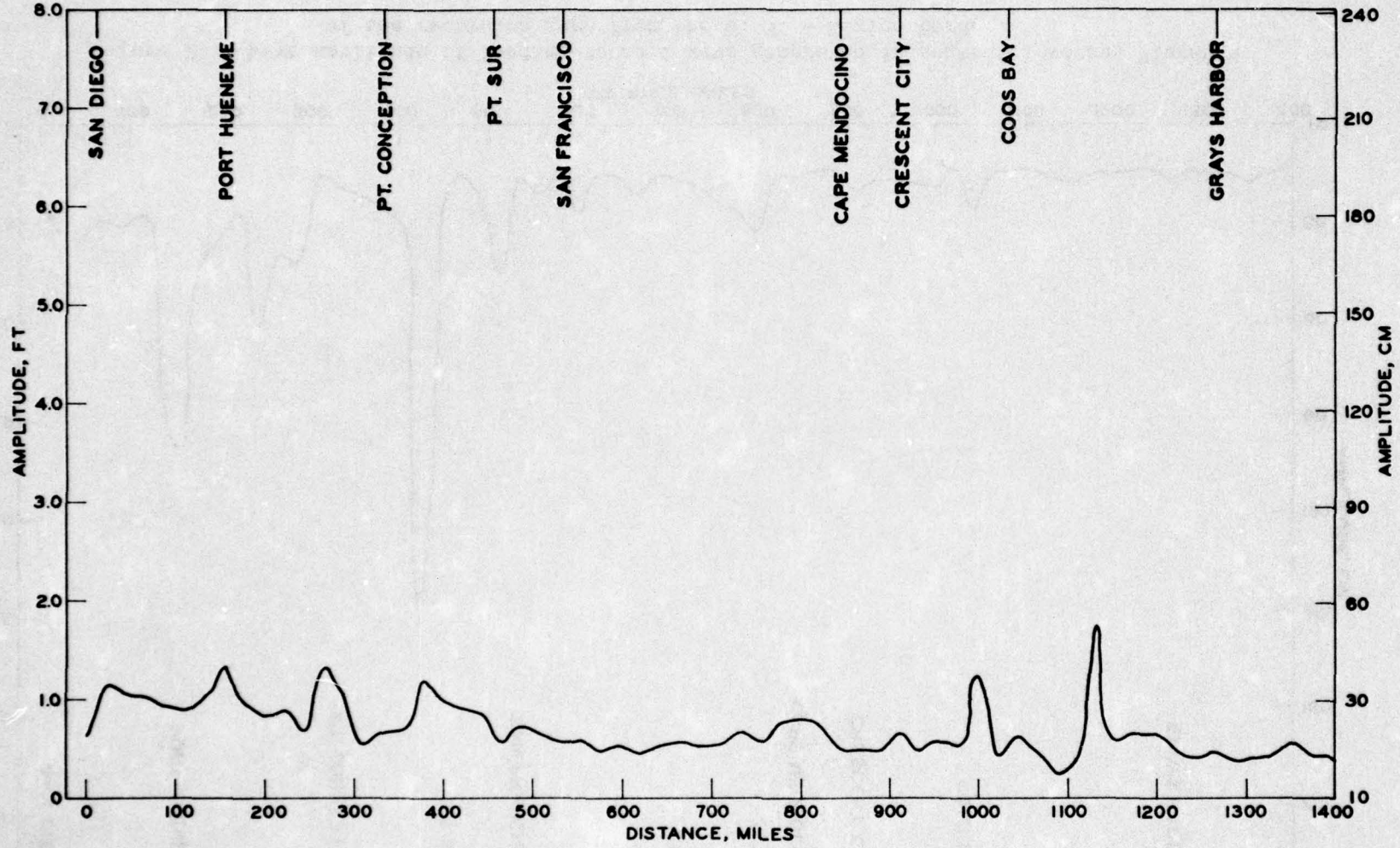

Figure 22. Wave amplitude of leading tsunami wave generated in segment 8 versus distance of the recording gage from the U. S. - Mexico border

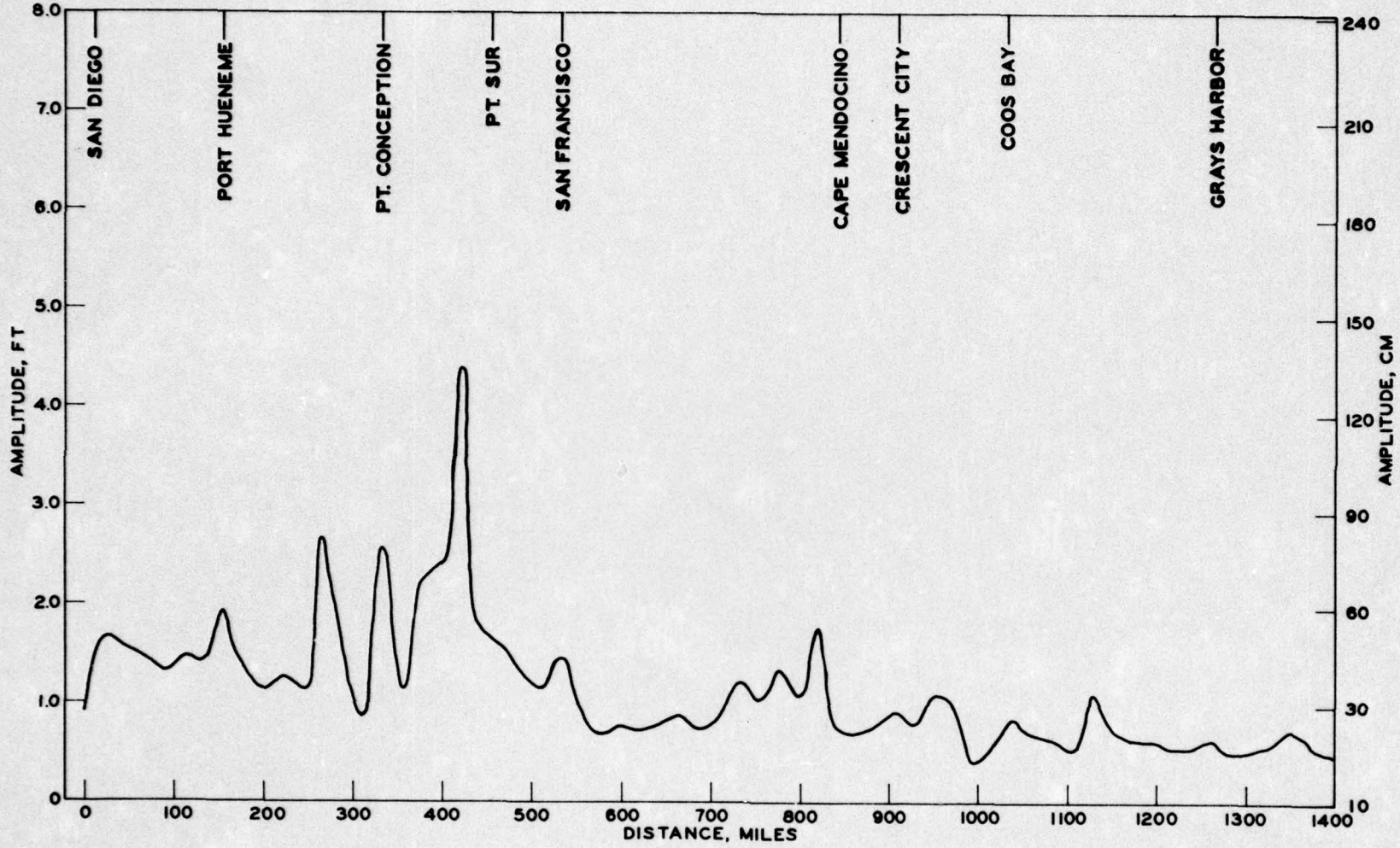

Figure 23. Wave amplitude of leading tsunami wave generated in segment 12 versus distance of the recording gage from the U. S. - Mexico border

APPENDIX A: NOTATION

a	Distance along x-axis, ft
A	Amplitude constant
b	Distance along x-axis, ft
C	Amplitude constant
d	Depth of water
d_a	Water depth a distance "a" from shore
g	Acceleration due to gravity
J_o	$J_o()$ Zeroth order Bessel function of the first kind
k	Variable, ft^{-1}
L	Wavelength
M_s	Surface wave magnitude
n	Refers to a time, $n\Delta t$
R_e	Radius of the earth
t	Time
U	Depth-averaged wave velocity component in the θ direction
U	Ursell number
V	Depth-averaged wave velocity component in the ϕ direction
x	Distance, ft
Δt	Length of a half-time step
ε	Phase factor
η	Wave elevation from reference water level
θ	Latitude measured positive from the north pole
ϕ	Longitude measured positive eastward from Greenwich
ω	Wave frequency, sec^{-1}
∂	Partial differential

In accordance with ER 70-2-3, paragraph 6c(1)(b), dated 15 February 1973, a facsimile catalog card in Library of Congress format is reproduced below.

Garcia, Andrew W

Effect of source orientation and location in the Peru-Chile Trench on tsunami amplitude along the Pacific Coast of the continental United States, by Andrew W. Garcia. Vicksburg, U. S. Army Engineer Waterways Experiment Station, 1976.

1 v. (various pagings) illus. 27 cm. (U. S. Waterways Experiment Station. Research report H-76-2)

Prepared for Office, Chief of Engineers, U. S. Army, Washington, D. C.

Includes bibliography.

1. Finite difference method. 2. Pacific Coast. 3. Peru-Chile Trench. 4. Tsunamis. I. U. S. Army. Corps of Engineers. (Series: U. S. Waterways Experiment Station, Vicksburg, Miss. Research report H-76-2)
TA7.W34r no.H-76-2